Euro. Jnl of Applied Mathematics (2020), *vol.* 31, *pp.* 871–917
doi:10.1017/S0956792519000305

Cops-on-the-dots: The linear stability of crime hotspots for a 1-D reaction-diffusion model of urban crime

ANDREAS BUTTENSCHOEN[1], THEODORE KOLOKOLNIKOV[2], MICHAEL J. WARD[1] and JUNCHENG WEI[1]

[1]*Department of Mathematics, UBC, Vancouver, Canada*
emails: abuttens@math.ubc.ca; ward@math.ubc.ca; jcwei@math.ubc.ca
[2]*Department of Mathematics and Statistics, Dalhousie, Halifax, Canada*
email: tkolokol@gmail.com

(*Received 31 October 2018*; *revised 4 October 2019*; *accepted 9 October 2019*; *first published online 11 November 2019*)

In a singularly perturbed limit, we analyse the existence and linear stability of steady-state hotspot solutions for an extension of the 1-D three-component reaction-diffusion (RD) system formulated and studied numerically in Jones et. al. [Math. Models. Meth. Appl. Sci., **20**, Suppl., (2010)], which models urban crime with police intervention. In our extended RD model, the field variables are the attractiveness field for burglary, the criminal population density and the police population density. Our model includes a scalar parameter that determines the strength of the police drift towards maxima of the attractiveness field. For a special choice of this parameter, we recover the 'cops-on-the-dots' policing strategy of Jones et. al., where the police mimic the drift of the criminals towards maxima of the attractiveness field. For our extended model, the method of matched asymptotic expansions is used to construct 1-D steady-state hotspot patterns as well as to derive nonlocal eigenvalue problems (NLEPs) that characterise the linear stability of these hotspot steady states to $\mathcal{O}(1)$ timescale instabilities. For a cops-on-the-dots policing strategy, we prove that a multi-hotspot steady state is linearly stable to synchronous perturbations of the hotspot amplitudes. Alternatively, for asynchronous perturbations of the hotspot amplitudes, a hybrid analytical–numerical method is used to construct linear stability phase diagrams in the police vs. criminal diffusivity parameter space. In one particular region of these phase diagrams, the hotspot steady states are shown to be unstable to asynchronous oscillatory instabilities in the hotspot amplitudes that arise from a Hopf bifurcation. Within the context of our model, this provides a parameter range where the effect of a cops-on-the-dots policing strategy is to only displace crime temporally between neighbouring spatial regions. Our hybrid approach to study the NLEPs combines rigorous spectral results with a numerical parameterisation of any Hopf bifurcation threshold. For the cops-on-the-dots policing strategy, our linear stability predictions for steady-state hotspot patterns are confirmed from full numerical PDE simulations of the three-component RD system.

Key words: Urban crime, hotspot patterns, nonlocal eigenvalue problem (NLEP), Hopf bifurcation, asynchronous oscillatory instability, cops-on-the-dots.

2010 Mathematics Subject Classification: Primary: 35K57; 35B25. Secondary: 35P.

1 Introduction

Motivated by the increased availability of residential burglary data, the development of mathematical modelling approaches to quantify and predict spatial patterns of urban crime was initiated in [18–20]. One primary feature incorporated into these models, which is based on observations from the available data (cf. [4]), is that spatial patterns of residential burglary are typically concentrated in small regions known as hotspots; a feature believed to be attributable to a repeat or near-repeat victimisation effect (cf. [9, 30]). There have been two primary frameworks that have been used to model the effect of police intervention on crime hotspot patterns. One approach, ideal for incorporating detailed real-world policing strategies, is large-scale simulations of agent-based models (cf. [5, 10]). However, with this approach, it is difficult to isolate the effect of changes in the model parameters. An alternative approach, more amenable to analysis, is to formulate PDE-based reaction-diffusion (RD) systems that model the police population density as an extra field variable (cf. [10, 15, 16]). More elaborate PDE models, such as in [31], formulate an optimal control strategy to minimise the overall crime rate by allowing the police to adapt to dynamically evolving crime patterns.

In our PDE-based approach, motivated by [10] and [16], the police intervention is modelled by a drift-diffusion PDE, in which we include a parameter that models the strength of the drift towards the maxima of the attractiveness field for burglary. For this three-component RD system consisting of an attractiveness field coupled to the criminal and police densities, we will study the existence and linear stability properties of steady-state hotspot patterns on a 1-D spatial domain $0 < x < S$ in a singularly perturbed limit. The specific non-dimensional three-component RD model of urban crime that we will analyse is formulated as

$$A_t = \epsilon^2 A_{xx} - A + \rho A + \alpha \,, \tag{1.1a}$$

$$\rho_t = D\left(\rho_x - 2\rho A_x/A\right)_x - \rho A + \gamma - \alpha - \rho U \,, \tag{1.1b}$$

$$\tau U_t = D\left(U_x - qUA_x/A\right)_x \,, \tag{1.1c}$$

where $A_x = \rho_x = U_x = 0$ at $x = 0, S$. Here A is the attractiveness field for burglary, while ρ and U are the densities of criminals and police, respectively, all of which are assumed to be non-negative. In this model, $\alpha > 0$ is the constant baseline attractiveness, $\gamma - \alpha > 0$ is the constant rate at which new criminals are introduced, D is the criminal diffusivity, $D_p \equiv D/\tau$ is the police diffusivity and $\epsilon \ll 1$ characterises the near-repeat victimisation effect (cf. [9, 18, 30]). For $q = 2$, this model is equivalent to that in [9]. For (1.1c), the total policing level $U_0 > 0$ is a prescribed constant given by

$$U_0 \equiv \int_0^S U(x,t)\,dx \,. \tag{1.2}$$

The integral $\int_0^S U(x,t)\,dx$ is a conserved quantity, independent of t, as is seen by integrating (1.1c) over the domain and using the no-flux boundary conditions. In (1.1), the other model parameters D, τ and q are all assumed to be positive constants.

In (1.1), the parameter $q > 0$ measures the degree of focus in the police patrol towards maxima of the attractiveness field. The choice $q = 2$, which recovers the PDE system derived and studied numerically in [10], is the 'cops-on-the-dots' strategy (cf. [10, 16]) where the police mimic the drift of the criminals towards maxima of A. In (1.1b), the police population density at a given

https://doi.org/10.1017/S0956792519000305 Published online by Cambridge University Press

spatial location decreases the local criminal population at a rate proportional to the local criminal population density (the $-\rho U$ term in (1.1b)). The resulting predator-prey type police interaction model (1.1) is to be contrasted with the 'simple police interaction' model formulated in [16], and analysed in [22], where the $-\rho U$ term in (1.1b) is replaced by $-U$.

In the absence of police, i.e. $U_0 = 0$, (1.1) reduces to the two-component PDE system for A and ρ first derived and studied in [18] and [20]. Pattern formation aspects for this 'basic' crime model have been well studied from various viewpoints, including, weakly nonlinear theory (cf. [19]), bifurcation theory near Turing bifurcation points (cf. [6, 8]) and the computation of global snaking-type bifurcation diagrams (cf. [13]), rigorous existence theory (cf. [17]), and asymptotic methods for constructing steady-state hotspot patterns whose linear stability properties can be analysed via NLEP theory (cf. [1, 11, 21]).

Our goal here is to extend the analysis given in [22] for the existence and linear stability of hotspot steady states for the simple police interaction model to the predator-prey type interaction model (1.1). We will show that the seemingly minor and innocuous replacement of $-U$ from the model in [22] with $-\rho U$ in (1.1b) leads to a significantly more challenging linear stability problem for hotspot equilibria. This is discussed in detail below.

As in [22] and [11], we will analyse (1.1) in the limit $\epsilon \to 0$ for the range $D = \mathcal{O}(\epsilon^{-2})$. Since $A(x) = \mathcal{O}(\epsilon^{-1})$ in the core of the hotspot near $x = 0$, it is convenient as in [22] to introduce the new variables v, u and $\mathcal{D}$ by

$$\rho = \epsilon^2 v A^2\,, \qquad U = uA^q\,, \qquad D = \epsilon^{-2}\mathcal{D}\,, \quad \text{so that} \quad D_p = \epsilon^{-2}\mathcal{D}/\tau\,. \tag{1.3}$$

In terms of A, v and u, on the domain $0 < x < S$, and with no-flux boundary conditions at $x = 0, S$, (1.1) transforms to

$$A_t = \epsilon^2 A_{xx} - A + \epsilon^2 v A^3 + \alpha\,, \tag{1.4a}$$

$$\epsilon^2 \left(A^2 v\right)_t = \mathcal{D}\left(A^2 v_x\right)_x - \epsilon^2 v A^3 + \gamma - \alpha - \epsilon^2 u v A^{2+q}\,, \tag{1.4b}$$

$$\tau\epsilon^2 \left(A^q u\right)_t = \mathcal{D}\left(A^q u_x\right)_x\,, \tag{1.4c}$$

In our analysis, we will assume that $\mathcal{D} = \mathcal{O}(1)$. Therefore, the asymptotic range of the police diffusivity D_p in (1.3) is determined by τ.

In Section 2, we use a formal singular perturbation analysis in the limit $\epsilon \to 0$ to construct hotspot steady-state solutions to (1.4) that have a common amplitude. Our steady-state analysis is restricted to the range $q > 1$, for which the police population density is asymptotically small in the background region away from the hotspots. In Proposition 2.1 and Corollary 2.2 below, we establish that steady-state hotspot solutions exist only when $U_0 < U_{0,\max} \equiv S(\gamma - \alpha)(q+1)/(2q)$.

In Section 3, we use a singular perturbation analysis combined with Floquet theory to derive two distinct NLEPs characterising the linear stability of hotspot steady states of (1.4) on the parameter range $\mathcal{O}(1) \ll D_p \ll \mathcal{O}(\epsilon^{-1-q})$ with $q > 1$. This analysis is similar to, but more intricate than, that given in [11] and [22]. One such NLEP, given below in Proposition 3.2, characterises the linear stability properties of a multi-hotspot steady-state solution, with $K \geq 2$ hotspots, to synchronous perturbations in the hotspot amplitudes. Alternatively, the second NLEP, given below in Proposition 3.4, characterises the linear stability properties of a multi-hotspot steady state, with $K \geq 2$ hotspots, to $K - 1 > 0$ different spatial modes of asynchronous

https://doi.org/10.1017/S0956792519000305 Published online by Cambridge University Press

perturbations of the hotspot amplitudes. A complicating feature in the analysis of these spectral problems, as compared to the analysis in [22], is that each of the two NLEPs has *three distinct nonlocal* terms consisting of a linear combination of $\int w^2\Phi$, $\int w^{q-1}\Phi$ and $\int w^{q+1}\Phi$. Here $w(y) = \sqrt{2}\,\mathrm{sech}\, y$ is the homoclinic profile of a hotspot and $\Phi(y)$ is the NLEP eigenfunction. As a result of this complexity, the determination of unstable spectra for these NLEPs is seemingly beyond the general NLEP stability theory with a single nonlocal term, as surveyed in [29]. For the simple police interaction model, studied in [22], the corresponding NLEPs had only two nonlocal terms.

In Section 4, we use a hybrid analytical–numerical strategy to determine the spectrum of the NLEP characterising the linear stability to synchronous perturbations. For arbitrary $q > 1$, the two different approaches developed in Sections 4.1 and 4.2 provide clear numerical evidence that this NLEP has no unstable eigenvalues. This strongly indicates that, for any $q > 1$ and D_p satisfying $\mathcal{O}(1) \ll D_p \ll \mathcal{O}(\epsilon^{-1-q})$, a one-hotspot steady state is always linearly stable and that a multi-hotspot steady state is always linearly stable to synchronous perturbations in the hotspot amplitudes. For the special case $q = 2$ of 'cops-on-the-dots', this linear stability conjecture is proved rigorously in Section 4.2.1. This proof of linear stability for $q = 2$ relies on some key identities that allow the NLEP with three nonlocal terms to be converted into an equivalent NLEP with a single nonlocal term.

For general $q > 1$, in Section 5, we determine the threshold value of $\mathcal{D}$ corresponding to a zero-eigenvalue crossing of the NLEP, as defined in Proposition 3.4, that characterises the linear stability of a multi-hotspot steady state to the asynchronous modes on the range $\mathcal{O}(1) \ll D_p \ll \mathcal{O}(\epsilon^{-1-q})$. For a K-hotspot steady state with $K \geq 2$, this critical value of $\mathcal{D}$, called the competition stability threshold, is

$$\mathcal{D}_c \equiv \frac{S}{8K^4\pi^2\alpha^2\left[1+\cos\left(\pi/K\right)\right]}\left[(1-q)\omega^3 + qS(\gamma-\alpha)\omega^2\right], \quad \text{where} \quad \omega \equiv S(\gamma-\alpha) - 2qU_0/(q+1), \tag{1.5}$$

on $U_0 < U_{0,\max} \equiv S(\gamma-\alpha)(q+1)/(2q)$. In the subregime $\mathcal{O}(\epsilon^{1-q}) \ll D_p \ll \mathcal{O}(\epsilon^{-1-q})$, a winding number analysis is used in Section 5.1 to prove, for an arbitrary $q > 1$, that a multi-hotspot steady state is linearly stable to asynchronous perturbations in the hotspot amplitudes if and only if $\mathcal{D} < \mathcal{D}_c$ (see Proposition 5.2 below).

For the special case $q = 2$ of 'cops-on-the-dots', in Section 6, we show how to transform the NLEP for the asynchronous modes into an equivalent NLEP with only one nonlocal term, which is then more readily analysed. With this reduction of the NLEP into a more standard form, which only applies when $q = 2$, in Proposition 6.4 we prove that a K-hotspot steady state, with $K \geq 2$, is always unstable to the asynchronous modes when $\mathcal{D} > \mathcal{D}_c$. Moreover, from a numerical parameterisation of branches of purely imaginary eigenvalues for this equivalent NLEP, we show that each of the $K-1$ asynchronous modes can undergo, on some intervals of $\mathcal{D}$, a Hopf bifurcation at critical values of the police diffusivity D_p on the range $D_p = \mathcal{O}(\epsilon^{-1})$. Overall, this hybrid approach provides phase diagrams in the ϵD_p vs. $\mathcal{D}$ parameter plane characterising the linear stability of the hotspot steady states to asynchronous perturbations in the hotspot amplitudes. Numerical evidence from PDE simulations suggests that hotspot amplitude oscillations arising from the Hopf bifurcation can be either subcritical or supercritical, depending on the parameter set. Linear stability phase diagrams for various U_0 are shown below in Figures 9 and 10 for $K = 2$ and $K = 3$, respectively. One key qualitative feature derived from these phase diagrams

https://doi.org/10.1017/S0956792519000305 Published online by Cambridge University Press

is that there is a region in the ϵD_p vs. $\mathcal{D}$ parameter space where the effect of police intervention is to only displace crime temporally between neighbouring spatial regions; a phenomenon qualitatively consistent with the field observations reported in [3] for a 'cops-on-the-dots' policing strategy.

As in [22], we emphasise that the interval in $\mathcal{D}$ where asynchronous hotspot amplitude oscillations occur disappears when $U_0 = 0$. Therefore, it is the third component of the RD system (1.4) that is needed to support these temporal oscillations. In contrast, for most two-component RD systems with localised spike-type solutions, such as the the Gray–Scott and Gierer–Meinhardt models (cf. [7, 12, 14, 24]), the dominant Hopf stability threshold for spike amplitude oscillations, based on an NLEP linear stability analysis, is determined by the spatial mode that synchronises the oscillations.

For $q = 2$, in Section 7, we validate the predictions of our linear stability analysis with full numerical PDE simulations of (1.4). Finally, in Section 8, we compare our linear stability results for (1.4) for a 'cops-on-the-dots' strategy with those in [22] for the simple police interaction model. We also briefly discuss some specific open problems and new directions warranting study.

2 Asymptotic construction of a multiple hotspot steady state

In the limit $\epsilon \to 0$, we use the method of matched asymptotic expansions to construct a steady-state solution to (1.4) on $0 \le x \le S$ with $K \ge 1$ interior hotspots of a common amplitude. We follow the approach in [22] in which we first construct a one-hotspot solution to (1.4) centred at $x = 0$ on the reference domain $|x| \le l$. From translation invariance, this construction yields a K interior hotspot steady-state solution on the original domain of length $S = (2\ell)K$. On $|x| \le \ell$, (1.2) yields that $\int_{-\ell}^{\ell} U\,dx = U_0/K$, where U_0 is the constant total police deployment.

On the reference domain $|x| \le l$, we centre a steady-state hotspot at $x = 0$, and we impose $A_x = v_x = u_x = 0$ at $x = \pm\ell$. For this *canonical* hotspot problem, the steady-state problem for (1.4) is to find $A(x)$, $v(x)$ and the constant u, satisfying

$$\epsilon^2 A_{xx} - A + \epsilon^2 v A^3 + \alpha = 0\,, \qquad |x| \le \ell\,; \qquad A_x = 0\,, \quad x = \pm\ell\,, \tag{2.1a}$$

$$\mathcal{D}\left(A^2 v_x\right)_x - \epsilon^2 v A^3 + \gamma - \alpha - \epsilon^2 u v A^{2+q} = 0\,, \qquad |x| \le \ell\,; \qquad v_x = 0\,, \quad x = \pm\ell\,, \tag{2.1b}$$

where the steady-state police population density $U(x)$ is related to u by

$$U = uA^q\,, \qquad \text{where} \qquad u = \frac{U_0}{K\int_{-\ell}^{\ell} A^q\,dx}\,. \tag{2.2}$$

For $\epsilon \to 0$, we have $A \sim \alpha + \mathcal{O}(\epsilon^2)$ in the outer region, while in the inner region near $x = 0$, we set $y = \epsilon^{-1}x$ and expand $A \sim \epsilon^{-1}A_0$ and $v \sim v_0$ in (2.1). To leading order, in the inner region, we obtain from (2.1) that

$$A_0 \sim \frac{w(y)}{\sqrt{v_0}}\,, \qquad v \sim v_0\,. \tag{2.3}$$

Here v_0 is a constant to be determined and $w(y) = \sqrt{2}\,\mathrm{sech}\,y$ is the homoclinic solution of

$$w'' - w + w^3 = 0\,, \qquad -\infty < y < \infty\,; \qquad w(0) > 0\,, \quad w'(0) = 0\,, \quad w \to 0 \quad \text{as} \quad y \to \pm\infty\,. \tag{2.4}$$

https://doi.org/10.1017/S0956792519000305 Published online by Cambridge University Press

Integrals of various powers of $w(y)$, as needed below, can be calculated in terms of the gamma function $\Gamma(z)$ by (see [22] and the appendix in [23])

$$\mathcal{I}_q \equiv \int_{-\infty}^{\infty} w^q \, dy = 2^{3q/2-1} \frac{[\Gamma(q/2)]^2}{\Gamma(q)} \,. \tag{2.5}$$

We will consider the range $q > 1$ where the dominant contribution to the integral $\int_{-\ell}^{\ell} A^q \, dx$ arises from the inner region:

$$\int_{-\ell}^{\ell} A^q \, dx \sim \epsilon^{1-q} v_0^{-q/2} \int_{-\infty}^{\infty} w^q \, dy = \mathcal{O}(\epsilon^{1-q}) \gg 1 \,.$$

Since $q > 1$, (2.2) shows that u depends, to leading order, only on the inner region contribution from A^q. For $\epsilon \ll 1$, we get

$$u \sim \epsilon^{q-1} \tilde{u}_e \,, \qquad \text{where} \qquad \tilde{u}_e \equiv \frac{U_0 v_0^{q/2}}{K \mathcal{I}_q} \,. \tag{2.6}$$

To determine v_0, we integrate (2.1b) over $-\ell < x < \ell$, while imposing $v_x(\pm\ell) = 0$. This yields that

$$\epsilon^2 \int_{-\ell}^{\ell} v A^3 \, dx = 2\ell \, (\gamma - \alpha) - \epsilon^2 u \int_{-\ell}^{\ell} v A^{2+q} \, dx \,. \tag{2.7}$$

Since $A \sim \alpha = \mathcal{O}(1)$ and $A = \mathcal{O}(\epsilon^{-1})$ in the outer and inner regions, respectively, it follows that, when $q > 1$, the dominant contribution to the integral arises from the inner region where $v \sim v_0$. In this way, and using (2.2) in (2.7), we get

$$\frac{\int_{-\infty}^{\infty} w^3 \, dy}{\sqrt{v_0}} \sim 2\ell \, (\gamma - \alpha) - \frac{\epsilon^2 U_0 v_0}{K} \frac{\int_{-\ell}^{\ell} A^{2+q} \, dx}{\int_{-\ell}^{\ell} A^q \, dx} \,. \tag{2.8}$$

Using $A \sim \epsilon^{-1} w(y)/\sqrt{v_0}$, together with (2.5), we calculate the integral ratio in (2.8) for $\epsilon \to 0$ as

$$\frac{\int_{-\ell}^{\ell} A^{2+q} \, dx}{\int_{-\ell}^{\ell} A^q \, dx} \sim \frac{\epsilon^{-2}}{v_0} \frac{\int_{-\infty}^{\infty} w^{q+2} \, dy}{\int_{-\infty}^{\infty} w^q \, dy} = \frac{\epsilon^{-2}}{v_0} \frac{2^{3(q+2)/2-1}}{2^{3q/2-1}} \left(\frac{\Gamma(1+q/2)}{\Gamma(q/2)} \right)^2 \frac{\Gamma(q)}{\Gamma(q+2)} = \frac{\epsilon^{-2}}{v_0} \frac{2q}{q+1} \,, \tag{2.9}$$

using $\Gamma(x+1) = x\Gamma(x)$. Then, by substituting (2.9) into (2.8), and using $\int_{-\infty}^{\infty} w^3 \, dy = \sqrt{2}\pi$, we observe that $\sqrt{v_0} > 0$ holds only when the total level U_0 of police deployment is below a threshold $U_{0,\max}$, i.e. when

$$U_0 < U_{0,\max} \equiv 2\ell K \, (\gamma - \alpha) \, \frac{(q+1)}{2q} = S(\gamma - \alpha) \frac{(q+1)}{2q} \,. \tag{2.10}$$

Here $S = 2\ell K$ is the original domain length. For this range of U_0, we can solve for v_0 to get

$$v_0 = 2\pi^2 \left[2\ell(\gamma - \alpha) - \frac{U_0}{K} \frac{2q}{q+1} \right]^{-2} \,. \tag{2.11}$$

https://doi.org/10.1017/S0956792519000305 Published online by Cambridge University Press

We conclude that a K-hotspot steady state exists when $U_0 < U_{0,\max}$. On this range of U_0, the amplitude of the hotspot, defined by $A_{\max} \equiv A(0) \gg 1$, is given by

$$A_{\max} \equiv A(0) \sim \epsilon^{-1} A_0(0) = \epsilon^{-1} \frac{w(0)}{\sqrt{v_0}} = \frac{\epsilon^{-1}\omega}{\pi K}, \qquad \text{where} \qquad \omega \equiv S(\gamma - \alpha) - U_0 \frac{2q}{q+1}. \tag{2.12}$$

We observe from (2.12) that the hotspot amplitude decreases with increasing K, U_0 or q.

To complete the asymptotic construction of the hotspot, in the outer region, we expand $v \sim v_e(x) + \dots$ and use $A \sim \alpha + \mathcal{O}(\epsilon^2)$. From (2.1b), we obtain to leading order that $v_e(x)$ satisfies

$$\mathcal{D} v_{exx} = -\frac{(\gamma - \alpha)}{\alpha^2}, \quad -\ell < x < \ell; \qquad v_e(0) = v_0, \qquad v_{ex}(\pm\ell) = 0, \tag{2.13}$$

which is readily solved analytically. We summarise our leading-order results for a steady-state K-hotspot pattern as follows:

Proposition 2.1 *Let $\epsilon \to 0$, $q > 1$ and $0 < U_0 < U_{0,max}$, where $U_{0,max}$ is given in (2.10). Then, (1.4) admits a steady-state solution on $(0, S)$ with K interior hotspots of a common amplitude. On each subdomain of length $2\ell = S/K$, and translated to $(-\ell, \ell)$ to contain exactly one hotspot at $x = 0$, the steady-state solution, to leading order, is given by*

$$A \sim \frac{w(x/\epsilon)}{\epsilon\sqrt{v_0}}, \quad \text{if} \quad x = \mathcal{O}(\epsilon); \qquad A \sim \alpha, \quad \text{if} \quad x = \mathcal{O}(1), \tag{2.14a}$$

$$v \sim v_e = \frac{\zeta}{2}\left[(\ell - |x|)^2 - \ell^2\right] + v_0, \qquad \text{where} \quad v_0 = 2\pi^2 K^2 \left[S(\gamma - \alpha) - U_0 \frac{2q}{q+1}\right]^{-2}, \tag{2.14b}$$

$$u \sim \epsilon^{q-1} \tilde{u}_e, \qquad \text{where} \quad \tilde{u}_e \equiv \frac{U_0 v_0^{q/2}}{K \mathcal{I}_q} \qquad \text{and} \quad \mathcal{I}_q \equiv \int_{-\infty}^{\infty} w^q \, dy = 2^{3q/2-1} \frac{[\Gamma(q/2)]^2}{\Gamma(q)}. \tag{2.14c}$$

Here, $w(y) = \sqrt{2}\,\mathrm{sech}\, y$ is the homoclinic of (2.4) and $\zeta \equiv -(\gamma - \alpha)/(\mathcal{D}\alpha^2)$.

In terms of the criminal and police densities, given by $\rho = \epsilon^2 v A^2$ and $U = u A^q$ from (1.3), we have the following:

Corollary 2.2 *Under the same conditions as in Proposition 2.1, (2.14) yields to leading order that*

$$A \sim \frac{w(x/\epsilon)}{\epsilon\sqrt{v_0}}, \quad \text{if} \quad x = \mathcal{O}(\epsilon); \qquad A \sim \alpha, \quad \text{if} \quad \mathcal{O}(\epsilon) \ll |x| < \ell, \tag{2.15a}$$

$$\rho \sim [w(x/\epsilon)]^2, \quad \text{if} \quad x = \mathcal{O}(\epsilon); \qquad \rho \sim \epsilon^2 v_e \alpha^2, \quad \text{if} \quad \mathcal{O}(\epsilon) \ll |x| < \ell, \tag{2.15b}$$

$$U \sim \frac{U_0}{\epsilon K \mathcal{I}_q}[w(x/\epsilon)]^q, \quad \text{if} \quad x = \mathcal{O}(\epsilon); \qquad U \sim \epsilon^{q-1}\alpha^q \frac{U_0 v_0^{q/2}}{K\mathcal{I}_q}, \quad \text{if} \quad \mathcal{O}(\epsilon) \ll |x| < \ell, \tag{2.15c}$$

where v_e and v_0 are given in (2.14) and $w(y) = \sqrt{2}\,\mathrm{sech}\, y$.

In Figure 1, we use (2.15) to plot the two-hotspot steady-state solution for a particular parameter set. This plot clearly shows the concentration behaviour of A, ρ and U near the hotspot locations.

https://doi.org/10.1017/S0956792519000305 Published online by Cambridge University Press

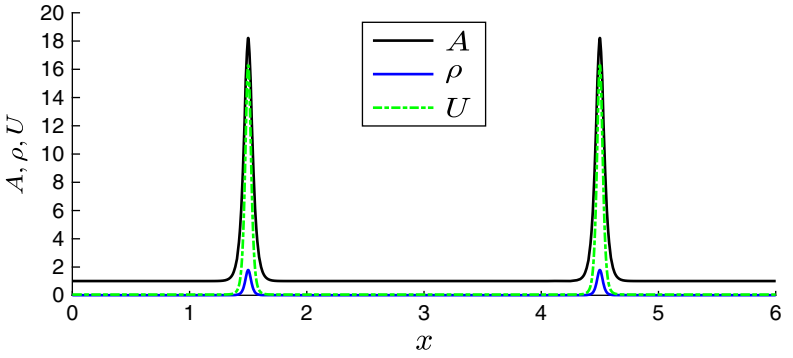

FIGURE 1. The steady-state two-hotspot solution for $S = 6$, $\gamma = 2$, $\alpha = 1$, $U_0 = 2$, $\epsilon = 0.03$, $\mathcal{D} = 0.3$, $D_p \approx 16.667$, for the 'cops-on-the-dots' $q = 2$ patrol, obtained from the asymptotic solution (2.15). These are the same parameter values used in the PDE simulations shown in the left panel of Figure 11 below.

From (2.15), we observe that the criminal population density near a hotspot is independent of the total police deployment U_0 and patrol focus q. Since $q > 1$, the police population density $U(x)$ is small in the outer region, but is asymptotically large near a hotspot.

We observe that our leading-order asymptotic result in (2.15) for the hotspot steady state is equivalent to simply replacing U_0 in Proposition 2.1 and Corollary 2.2 of [22] with $2qU_0/(q+1)$. Since $2q/(q+1) > 1$ for $q > 1$, we conclude that, for the same parameter values and level U_0 of total police deployment, the steady-state hotspot amplitude is smaller for the RD model (1.4) with predator-prey type police interaction than for the RD model of [22] with simple police interaction.

3 The NLEP for a K-hotspot steady-state pattern

To analyse the linear stability of a K-hotspot steady-state solution, we must extend the singular perturbation approach used in [22] to derive the corresponding nonlocal eigenvalue problem (NLEP). This is done by first deriving the NLEP for a one-hotspot solution on the reference domain $|x| \le \ell$, subject to Floquet-type boundary conditions imposed at $x = \pm\ell$. In terms of this canonical problem, the NLEP for the finite domain problem $0 < x < S$ with Neumann conditions at $x = 0, S$ is then readily recovered as in [22] (see also [11]). Since the analysis to derive the NLEP is similar to that in [22], we only outline it below. Further details on the derivation of the NLEP are given in Appendix A.

3.1 Linearisation with Floquet boundary conditions

Let (A_e, v_e, u_e) denote the steady state with a single hotspot centred at $x = 0$ in $|x| \le \ell$. We introduce the perturbation

$$A = A_e + e^{\lambda t}\phi\,, \qquad v = v_e + e^{\lambda t}\epsilon\psi\,, \qquad u = u_e + e^{\lambda t}\epsilon^q\eta\,, \tag{3.1}$$

where the asymptotic orders of the perturbations ($\mathcal{O}(1)$, $\mathcal{O}(\epsilon)$ and $\mathcal{O}(\epsilon^q)$) are chosen so that ϕ, ψ and η are all $\mathcal{O}(1)$ in the inner region. By substituting (3.1) into (1.4) and linearising, we obtain that

https://doi.org/10.1017/S0956792519000305 Published online by Cambridge University Press

$$\epsilon^2\phi_{xx} - \phi + 3\epsilon^2 v_e A_e^2\phi + \epsilon^3 A_e^3\psi = \lambda\phi\,, \tag{3.2a}$$

$$\begin{aligned}\mathcal{D}\left(2A_e v_{ex}\phi + \epsilon A_e^2\psi_x\right)_x - 3\epsilon^2 A_e^2 v_e\phi - \epsilon^3 A_e^3\psi - \epsilon^2(2+q)u_e v_e A_e^{q+1}\phi \\ -\epsilon^{2+q} v_e A_e^{2+q}\eta - \epsilon^3 u_e A_e^{2+q}\psi = \lambda\epsilon^2\left(2A_e v_e\phi + \epsilon A_e^2\psi\right)\,,\end{aligned} \tag{3.2b}$$

$$\mathcal{D}\left(qA_e^{q-1}u_{ex}\phi + \epsilon^q A_e^q\eta_x\right)_x = \epsilon^2\tau\lambda\left(qA_e^{q-1}u_e\phi + \epsilon^q A_e^q\eta\right)\,. \tag{3.2c}$$

As in [22], for $K \geq 2$, we impose Floquet-type boundary conditions at $x = \pm\ell$ for ψ, η, and ϕ:

$$\begin{pmatrix}\eta(\ell)\\ \psi(\ell)\\ \phi(\ell)\end{pmatrix} = z\begin{pmatrix}\eta(-\ell)\\ \psi(-\ell)\\ \phi(-\ell)\end{pmatrix}, \qquad \begin{pmatrix}\eta_x(\ell)\\ \psi_x(\ell)\\ \phi_x(\ell)\end{pmatrix} = z\begin{pmatrix}\eta_x(-\ell)\\ \psi_x(-\ell)\\ \phi_x(-\ell)\end{pmatrix}. \tag{3.3}$$

Here z is a complex-valued parameter. Since ϕ is localised near the core of the hotspot, it is only the Floquet-type boundary condition for the long-range components η and ψ that is essential to the analysis below. We will consider the case of a single hotspot, where $K = 1$, separately in Section 3.2 below.

For $K \geq 2$, the NLEP associated with a K-hotspot pattern on $[-l, (2K-1)l]$ with *periodic boundary conditions*, on a domain of length $2Kl$, is obtained by setting $z^K = 1$, which yields $z_j = e^{2\pi ij/K}$ for $j = 0, \ldots, K-1$. For these values of z_j in (3.3), we obtain the spectral problem for the linear stability of a K-hotspot solution on a domain of length $2Kl$ with periodic boundary conditions. To relate the spectra of the periodic problem to the Neumann problem, in such a way that the Neumann problem is still posed on a domain of length S, we proceed as in Section 3 of [22] (see also Section 3 of [11] and the appendix of [23]). There it was shown that we need only to replace $2K$ with K in the definition of z_j. In this way, the Floquet parameters in (3.3) for a hotspot steady state on a domain of length $S = 2lK$ having $K \geq 2$ interior hotspots and Neumann boundary conditions at $x = 0$ and $x = S$ is $z = z_j \equiv e^{\pi ij/K}$ for $j = 0, \ldots, K-1$. For these values of z, the following identity is needed below:

$$\frac{(z-1)^2}{2z} = \mathrm{Re}(z) - 1 = \cos\left(\frac{\pi j}{K}\right) - 1\,, \qquad j = 0, \ldots, K-1\,. \tag{3.4}$$

We now begin our derivation of the NLEP. For (3.2a), in the inner region where $A_e \sim \epsilon^{-1}w/\sqrt{v_0}$, $v_e \sim v_0$, we have that $\psi \sim \psi(0) \equiv \psi_0$. It follows that the leading-order term $\Phi(y) = \phi(\epsilon y)$ in the inner expansion of ϕ satisfies

$$\Phi'' - \Phi + 3w^2\Phi + \frac{\psi(0)}{v_0^{3/2}}w^3 = \lambda\Phi\,. \tag{3.5}$$

In the outer region $\epsilon \ll |x| \leq \ell$, to leading order, we obtain from (3.2) that

$$\phi \sim \epsilon^3\alpha^3\psi/[\lambda + 1 - 3\epsilon^2\alpha^2 v_e] = \mathcal{O}(\epsilon^3), \qquad \psi_{xx} \approx 0\,, \qquad \eta_{xx} \approx 0\,. \tag{3.6}$$

The goal of the calculation below is to determine $\psi(0)$, which from (3.5) yields the NLEP. To do so, we must derive appropriate jump conditions for ψ_x and η_x across the hotspot region centred at $x = 0$. This calculation, summarised in Appendix A, then leads to linear boundary value problems (BVPs) for ψ and η, from which we can calculate $\psi(0)$.

https://doi.org/10.1017/S0956792519000305 Published online by Cambridge University Press

As shown in Appendix A, we obtain that the outer approximation for $\psi(x)$ satisfies

$$\psi_{xx} = 0\,, \quad |x| \le \ell\,; \quad e_0\,[\psi_x]_0 = e_1\psi(0) + e_2\eta(0) + e_3\,, \quad \psi(\ell) = z\psi(-\ell)\,, \quad \psi_x(\ell) = z\psi_x(-\ell)\,, \tag{3.7a}$$

where we have defined $[a]_0 \equiv a(0^+) - a(0^-)$. Defining $\int (\dots) \equiv \int_{-\infty}^{\infty} (\dots)\, dy$, the coefficients e_j, for $j = 0, \dots, 3$, are

$$\begin{aligned} e_0 &\equiv \mathcal{D}\alpha^2\,, \qquad e_1 \equiv \frac{1}{v_0^{3/2}} \int w^3 + \frac{\tilde{u}_e}{v_0^{1+q/2}} \int w^{q+2}\,, \\ e_2 &\equiv \frac{1}{v_0^{q/2}} \int w^{2+q}\,, \qquad e_3 \equiv 3\int w^2\Phi + \frac{\tilde{u}_e}{v_0^{(q-1)/2}}(q+2)\int w^{q+1}\Phi\,. \end{aligned} \tag{3.7b}$$

The BVP (3.7) is defined in terms of $\eta(0)$, which must be found from a separate BVP (see Appendix A). In Appendix A, we show that on the range

$$\mathcal{O}(\epsilon^{q-1}) \ll \tau \ll \mathcal{O}(\epsilon^{-2}) \qquad \text{so that} \qquad \mathcal{O}(1) \ll D_p \ll \mathcal{O}(\epsilon^{-q-1})\,, \tag{3.8}$$

we have that $\eta(0)$ is determined from the following leading-order BVP:

$$\eta_{xx} = 0\,, \quad |x| \le \ell\,; \qquad d_0\,[\eta_x]_0 = d_1\eta(0) + d_2\,, \quad \eta(\ell) = z\eta(-\ell)\,, \quad \eta_x(\ell) = z\eta_x(-\ell)\,. \tag{3.9a}$$

In terms of v_0 and $\tilde{u}_e$, as defined in (2.14), the constants d_0, d_1 and d_2, are defined by

$$d_0 \equiv \mathcal{D}\alpha^q, \qquad d_1 \equiv \frac{\hat{\tau}\lambda}{v_0^{q/2}} \int w^q, \qquad d_2 \equiv \frac{\hat{\tau}\lambda q\tilde{u}_e}{v_0^{(q-1)/2}} \int w^{q-1}\Phi\,. \tag{3.9b}$$

Here we have defined $\hat{\tau}$ by

$$\hat{\tau} \equiv \epsilon^{3-q}\tau\,. \tag{3.10}$$

In view of (3.8), the BVP (3.9a) for $q > 1$ holds on the following range of $\hat{\tau}$:

$$\mathcal{O}(\epsilon^2) \ll \hat{\tau} \ll \mathcal{O}(\epsilon^{1-q})\,, \qquad \text{where} \qquad D_p = \epsilon^{1-q}\mathcal{D}/\hat{\tau}\,. \tag{3.11}$$

To calculate $\psi(0)$ and $\eta(0)$, we need the following simple result, as proved in Lemma 3.1 of [22]:

Lemma 3.1 *(Lemma 3.1 of [22]) For $|x| < \ell$, suppose that $y(x)$ satisfies*

$$y_{xx} = 0\,, \quad -\ell < x < \ell\,; \qquad f_0\,[y_x]_0 = f_1 y(0) + f_2\,; \qquad y(\ell) = zy(-\ell)\,, \quad y_x(\ell) = zy_x(-\ell)\,, \tag{3.12}$$

where f_0, f_1 and f_2, are non-zero constants, and let z satisfy (3.4). Then, $y(0)$ is given by

$$y(0) = f_2\left[\frac{f_0}{\ell}\frac{(z-1)^2}{2z} - f_1\right]^{-1} = -\frac{f_2}{f_0[1-\cos(\pi j/K)]/\ell + f_1}\,. \tag{3.13}$$

Lemma 3.1 with $f_0 = e_0, f_1 = e_1$ and $f_2 = e_2\eta(0) + e_3$ yields $\psi(0)$ from (3.7). Similarly, $\eta(0)$ is found from (3.9) using Lemma 3.1 with $f_0 = d_0, f_1 = d_1$ and $f_2 = d_2$. In this way, we get

$$\psi(0) = -\frac{e_2\eta(0) + e_3}{e_0[1-\cos(\pi j/K)]/\ell + e_1}\,, \qquad \text{and} \qquad \eta(0) = -\frac{d_2}{d_0[1-\cos(\pi j/K)]/\ell + d_1}\,. \tag{3.14}$$

https://doi.org/10.1017/S0956792519000305 Published online by Cambridge University Press

Upon combining these two results, and using (3.7b) and (3.9b) for e_0 and d_0, respectively, we determine $\psi(0)$ as

$$\psi(0) = -\frac{1}{\mathcal{D}_j\alpha^2 + e_1}\left[e_3 - \frac{e_2 d_2}{\mathcal{D}_j\alpha^q + d_1}\right], \tag{3.15}$$

where we have defined $\mathcal{D}_j$, which satisfies $\mathcal{D}_j < \mathcal{D}_{j+1}$ for any $j = 0, \ldots, K-2$, by

$$\mathcal{D}_j \equiv \frac{\mathcal{D}}{\ell}\left[1 - \cos\left(\frac{\pi j}{K}\right)\right], \qquad j = 0, \ldots, K-1\,, \quad \text{where} \quad l = \frac{S}{2K}\,. \tag{3.16}$$

To determine the coefficient $\psi(0)/v_0^{3/2}$ in (3.5) in terms of the original parameters, which will yield the NLEP, we next need to simplify the expressions for e_1, e_2, e_3, d_1 and d_2 in (3.7b) and (3.9b), using (2.6) for $\tilde{u}_e$ and an explicit formula for the integral ratio $\int w^{q+2}/\int w^q$, as given in (2.9). A short calculation yields that

$$e_1 = \frac{\int w^3}{v_0^{3/2}} + \frac{2qU_0}{(q+1)Kv_0}\,, \qquad e_2 = \frac{\int w^{q+2}}{v_0^{q/2}}\,, \qquad e_3 = 3\int w^2\Phi + \frac{U_0\sqrt{v_0}}{K}(q+2)\frac{\int w^{q+1}\Phi}{\int w^q}\,, \tag{3.17a}$$

$$d_1 = \hat{\tau}\lambda\frac{\int w^q}{v_0^{q/2}}, \qquad d_2 = \hat{\tau}\lambda q\left(\frac{U_0\sqrt{v_0}}{K}\right)\frac{\int w^{q-1}\Phi}{\int w^q}\,. \tag{3.17b}$$

Upon substituting (3.17) into (3.15), we obtain, after some algebra, that

$$-\frac{\psi(0)}{v_0^{3/2}} = \chi_{0j}\left(3\frac{\int w^2\Phi}{\int w^3}\right) + \chi_{1j}\left((q+2)\frac{\int w^{q+1}\Phi}{\int w^{q+2}}\right) + \chi_{2j}\left(q\frac{\int w^{q-1}\Phi}{\int w^q}\right), \tag{3.18a}$$

where we have defined

$$\chi_{0j} \equiv \frac{1}{1 + \kappa_q + v_0^{3/2}\mathcal{D}_j\alpha^2/\int w^3}\,, \qquad \chi_{1j} \equiv \chi_{0j}\kappa_q\,, \qquad \chi_{2j} \equiv -\chi_{0j}\left(\frac{\hat{\tau}\lambda\kappa_q}{\hat{\tau}\lambda + \mathcal{D}_j\alpha^q v_0^{q/2}/\int w^q}\right). \tag{3.18b}$$

Here κ_q is defined by

$$\kappa_q \equiv \frac{U_0\sqrt{v_0}}{K\int w^3}\frac{\int w^{q+2}}{\int w^q} = \frac{2qU_0}{\omega(q+1)}\,, \qquad \text{where} \qquad \omega \equiv S(\gamma - \alpha) - \frac{2qU_0}{q+1}\,. \tag{3.19}$$

In calculating κ_q above, we evaluated the integral ratio in (3.19) using (2.9) and then recalled (2.14) for v_0. We observe from (3.19) that as U_0 tends to the maximum policing level $U_{0,\max}$ for which a steady state exists, then $\omega \to 0^+$ and correspondingly $\kappa_q \to \infty$.

From (3.18b), we first derive the NLEP for the mode $j = 0$, which corresponds to synchronous perturbations of the hotspot amplitudes. For this mode, we have $\mathcal{D}_0 = 0$ from (3.16). Therefore, from (3.18b), the coefficients reduce to $\chi_{00} = 1/(1+\kappa_q)$, $\chi_{10} = \kappa_q/(1+\kappa_q)$ and $\chi_{20} = -\kappa_q/(1+\kappa_q)$. With these values, we substitute (3.18a) into (3.5) to obtain the following NLEP for the synchronous mode:

Proposition 3.2 *Let $\epsilon \to 0$, $K \geq 2$, $q > 1$ and $0 < U_0 < U_{0,max} = (q+1)S(\gamma-\alpha)/(2q)$, and assume that $\mathcal{D} = \epsilon^2 D = \mathcal{O}(1)$ and $\mathcal{O}(1) \ll D_p \ll \mathcal{O}(\epsilon^{-q-1})$. Then, the linear stability on an $\mathcal{O}(1)$*

https://doi.org/10.1017/S0956792519000305 Published online by Cambridge University Press

timescale of a K-hotspot steady-state solution for (1.4) to synchronous perturbations of the hotspot amplitudes is determined by the spectrum of the following NLEP for $\Phi(y) \in L^2(\mathbb{R})$*:*

$$L_0\Phi - \frac{w^3}{1+\kappa_q}\left[3\frac{\int w^2\Phi}{\int w^3} + \kappa_q(q+2)\frac{\int w^{q+1}\Phi}{\int w^{q+2}} - \kappa_q q\frac{\int w^{q-1}\Phi}{\int w^q}\right] = \lambda\Phi\,, \tag{3.20}$$

where $L_0\Phi \equiv \Phi'' - \Phi + 3w^2\Phi$ *and* κ_q *is defined by* $\kappa_q = 2qU_0/[\omega(q+1)]$*, where* $\omega \equiv S(\gamma - \alpha) - 2qU_0/(q+1)$.

We remark that the NLEP (3.20) for the synchronous mode depends only on κ_q and is independent of the criminal and police diffusivities characterised by $\mathcal{D}$ and $\hat{\tau}$, respectively.

Remark 3.3 *In Section 3.2, we show that the NLEP in (3.20) also governs the linear stability of a one-hotspot steady-state solution.*

Next, we consider the asynchronous modes where $j = 1, \dots, K-1$. For these modes, in order to obtain an NLEP with as few bifurcation parameters as possible, we introduce in (3.18b) two additional rescaled parameters $\mathcal{D}_u$ and τ_u defined by

$$\mathcal{D}_j = \frac{\int w^3}{v_0^{3/2}\alpha^2}\mathcal{D}_u\,, \qquad \hat{\tau} = \mathcal{D}_j\alpha^q\frac{v_0^{q/2}}{\int w^q}\tau_u\,. \tag{3.21}$$

Using (3.21) in (3.18), an NLEP is obtained by substituting (3.18a) into (3.5). The result is summarised as follows:

Proposition 3.4 *Let* $\epsilon \to 0$*,* $K \geq 2$*,* $q > 1$*,* $0 < U_0 < U_{0,max} = (q+1)S(\gamma-\alpha)/(2q)$*,* $\mathcal{D} = \epsilon^2 D = \mathcal{O}(1)$ *and* $\mathcal{O}(1) \ll D_p \ll \mathcal{O}(\epsilon^{-q-1})$*. Then, the linear stability on an* $\mathcal{O}(1)$ *timescale of a K-hotspot steady-state solution for (1.4) for the asynchronous modes* $j = 1, \dots, K-1$ *is characterised by the spectrum of the following NLEP for* $\Phi(y) \in L^2(\mathbb{R})$*:*

$$L_0\Phi - \chi_0 w^3\left(3\frac{\int w^2\Phi}{\int w^3}\right) - \chi_1 w^3\left((q+2)\frac{\int w^{q+1}\Phi}{\int w^{q+2}}\right) - \chi_2 w^3\left(q\frac{\int w^{q-1}\Phi}{\int w^q}\right) = \lambda\Phi\,, \tag{3.22a}$$

where $L_0\Phi \equiv \Phi'' - \Phi + 3w^2\Phi$ *and* $w = \sqrt{2}\,\mathrm{sech}\, y$ *is the homoclinic of (2.4). Here the coefficients of the multipliers are*

$$\chi_0 = \frac{1}{1+\kappa_q+\mathcal{D}_u}\,, \quad \chi_1 = \chi_0\kappa_q\,, \quad \chi_2 = -\chi_0\kappa_q\frac{\tau_u\lambda}{1+\tau_u\lambda}\,; \qquad \kappa_q = \frac{2q}{q+1}\frac{U_0}{\omega}\,, \quad \omega \equiv S(\gamma-\alpha) - \frac{2q}{q+1}U_0\,. \tag{3.22b}$$

For a given $q > 1$, the spectrum of the NLEP (3.22) depends on the three key parameters $\mathcal{D}_u$, τ_u and κ_q. To relate these parameters to the original criminal diffusivity $\mathcal{D}$, we use (3.21) and (3.16), and then (2.14) for v_0 to get

$$\mathcal{D} = \left(\frac{\int w^3}{\alpha^2 v_0^{3/2}}\right)\frac{S}{2K\left[1-\cos\left(\frac{\pi j}{K}\right)\right]}\mathcal{D}_u = \frac{\omega^3 S}{4K^4\pi^2\alpha^2\left[1-\cos\left(\frac{\pi j}{K}\right)\right]}\mathcal{D}_u\,, \qquad j = 1, \dots, K-1\,, \tag{3.23}$$

https://doi.org/10.1017/S0956792519000305 Published online by Cambridge University Press

where ω is defined in (3.22b). In addition, to map τ_u to the original police diffusivity D_p, we simply substitute (3.21) for $\hat{\tau}$ into (3.11) for D_p and use (3.16) for $\mathcal{D}_j$ and (2.14) for v_0. In this way, for $K \geq 2$, we obtain

$$D_p = \frac{S\int w^q}{2K\alpha^q\left[1-\cos\left(\frac{\pi j}{K}\right)\right]}\left(\frac{\omega}{K\int w^3}\right)^q\left(\frac{\epsilon^{1-q}}{\tau_u}\right), \qquad j=1,\ldots,K-1\,. \tag{3.24}$$

Remark 3.5 *In view of (3.11) and (3.21) relating $\hat{\tau}$ and τ_u, the NLEP (3.22) holds not only when $\tau_u = \mathcal{O}(1)$ but for the entire range $\mathcal{O}(\epsilon^2) \ll \tau_u \ll \mathcal{O}(\epsilon^{1-q})$. Since $q > 1$, this implies that we can consider the limiting cases $\tau_u \to 0^+$ and $\tau_u \to \infty$ in (3.22), with the interpretation that $\tau_u \gg \mathcal{O}(\epsilon^2)$ and $\tau_u \ll \mathcal{O}(\epsilon^{1-q})$, respectively.*

We refer to the NLEP (3.22) as a *universal* NLEP, since we need only to determine, with respect to the bifurcation parameters $\mathcal{D}_u$, τ_u and κ_q, when all discrete eigenvalues of (3.22) satisfy $\mathrm{Re}(\lambda) \leq 0$. The regions of linear stability with respect to these key parameters can then be mapped to corresponding regions of stability with respect to the original parameters $\mathcal{D}$ and D_p (for a given U_0, S, γ, α and q) using (3.23) and (3.24). Correspondingly, we will also identify parameter ranges for which the NLEP predicts instabilities owing to it having a discrete eigenvalue in $\mathrm{Re}(\lambda) > 0$.

3.2 Derivation of the NLEP for a single hotspot: $K = 1$ case

To derive an NLEP for the case of a single hotspot, we simply impose Neumann boundary conditions directly at $x = \pm\ell$ in (3.7) and (3.9). This yields that $\psi(x) = \psi(0)$ and $\eta(x) = \eta(0)$ on $|x| \leq \ell$. From (3.9) and (3.7), we conclude that

$$\eta(0) = -\frac{d_2}{d_1} \qquad \psi(0) = -\frac{1}{e_1}\left(e_2\eta(0)+e_3\right) = -\frac{1}{e_1}\left(e_3 - \frac{e_2 d_2}{d_1}\right).$$

Using the explicit expressions for the coefficients given in (3.17), we calculate $\psi(0)/v_0^{3/2}$, which leads to the NLEP from (3.5). In this way, we obtain that the NLEP for a single hotspot is also given by (3.20) of Proposition 3.2.

4 No unstable eigenvalues for the NLEP (3.20) for the synchronous mode

In this section, we study the NLEP (3.20) of Proposition 3.2, which applies to either amplitude perturbations of a one-hotspot steady state or synchronous perturbations of the amplitudes of a multi-hotspot steady state.

4.1 Numerical computations

We first show numerically that (3.20) has no unstable eigenvalues for any $\kappa_q \geq 0$ and $q > 1$. To do so, we write (3.20) as

$$L_0\Phi - w^3\left(a\int w^{q+1}\Phi + b\int w^2\Phi + c\int w^{q-1}\Phi\right) = \lambda\Phi\,, \tag{4.1}$$

https://doi.org/10.1017/S0956792519000305 Published online by Cambridge University Press

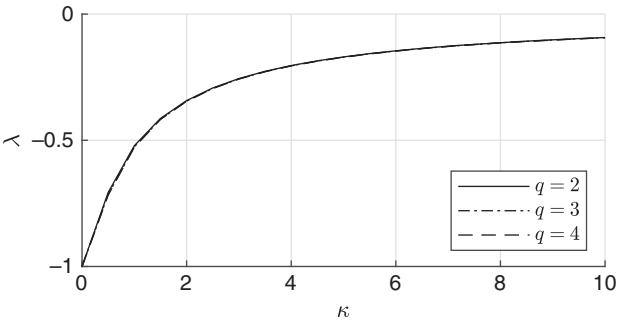

FIGURE 2. Numerical approximation of the principal eigenvalue of (4.1) for $q = 2$, $q = 3$ and $q = 4$, with $\kappa \in (0, 10)$. We observe that $\lambda < 0$ in all cases, and that the principal eigenvalue is rather insensitive to changes in q as the curves are almost overlapping.

where the constants a, b and c are defined by

$$a = \frac{\kappa_q\,(q+2)}{\left(1+\kappa_q\right)\int w^{q+2}}\,, \qquad b = \frac{3}{\left(1+\kappa_q\right)\int w^3}\,, \qquad c = -\frac{q\kappa_q}{\left(1+\kappa_q\right)\int w^q}\,. \tag{4.2}$$

To numerically compute the discrete eigenvalues of (4.1), we convert this NLEP into a linear algebra problem using finite differences. As we are interested only in even solutions, we consider (4.1) on $[0, \infty]$. Since $w(y)$ decays exponentially as $y \to +\infty$, we truncate the positive half-line to the large interval $x \in [0, L]$, where we chose $L = 20$ (decreasing L to 10 changes the results below by less than 0.01%). We discretise $\Phi(x_j) \sim \Phi_j$ where $x_j = j\Delta x$, for $j = 0 \ldots N-1$ and $\Delta x = L/(N-1)$, with $N = 100$. Increasing N to 200 changed the results below by less than 1%. We use standard centred differences to approximate Φ'' and the trapezoid rule to approximate integrals in (4.1). In this way, we obtain the matrix eigenvalue problem $\mathcal{M}\boldsymbol{\Phi} = \lambda\boldsymbol{\Phi}$, where $\boldsymbol{\Phi} \equiv (\Phi_1, \ldots, \Phi_N)^T$. The eigenvalue of $\mathcal{M}$ with the largest real part then provides an excellent approximation to the principal eigenvalue of (4.1).

In terms of κ_q, this numerical approximation of the principal eigenvalue of (4.1) is plotted for $q = 2$, $q = 3$ and $q = 4$ in Figure 2. The results shown in Figure 2 suggest that (3.20) has no unstable eigenvalues for any $\kappa_q \geq 0$ and $q \geq 1$. Although the NLEP (3.20) is only relevant to the stability of a hotspot steady state only when $q > 1$, as a partial confirmation of the numerical results in Figure 2, we now show how to determine λ analytically from (4.1) when $q = 1$.

Let Φ and λ be any eigenpair of (4.1) for which $\int w^2\Phi \neq 0$ and $\int \Phi \neq 0$. We multiply (4.1) by w^2 and integrate. Using the identity $L_0 w^2 = 3w^2$, we obtain

$$(\lambda - 3)\int w^2\Phi = -(a+b)\int w^5 \int w^2\Phi - c\int w^5 \int \Phi\,. \tag{4.3}$$

Next, we integrate (4.1) upon recalling $L_0\Phi = \Phi'' - \Phi + 3w^2\Phi$. This yields

$$(\lambda + 1)\int \Phi = 3\int w^2\Phi - \int w^3\left[(a+b)\int w^2\Phi + c\int \Phi\right]. \tag{4.4}$$

By eliminating $\int \Phi w^2$ and $\int \Phi$ from (4.3) and (4.4), we then obtain the following quadratic equation for λ:

$$c\int w^5\left(3 - (a+b)\int w^3\right) + \left(\lambda - 3 + (a+b)\int w^5\right)\left(c\int w^3 + \lambda + 1\right) = 0\,. \tag{4.5}$$

https://doi.org/10.1017/S0956792519000305 Published online by Cambridge University Press

For $q=1$, we obtain from (4.2) that $a+b=3/\int w^3$ and $c=-\kappa_1/\left[(1+\kappa_1)\int w\right]$. Upon substituting these expressions into (4.5), and using $\int w^3/\int w=1$ and $\int w^5/\int w^3=3/2$, we get

$$\left(\lambda+\frac{1}{1+\kappa_1}\right)\left(\lambda+\frac{3}{2}\right)=0\,. \tag{4.6}$$

Since $\kappa_1\geq 0$, we conclude that the principal eigenvalue of (4.1) when $q=1$ is

$$\lambda=-\frac{1}{1+\kappa_1}. \tag{4.7}$$

Setting $\kappa_1=1$ gives $\lambda=-1/2$, which agrees with the numerical result arising from a discretisation of (4.1) (not shown).

4.2 A hybrid analytical–numerical approach

We now give an alternative approach that provides a sufficient condition to ensure that the NLEP (3.20) has no unstable eigenvalues. This sufficient condition is then investigated numerically. For this hybrid analytical–numerical approach, we write the NLEP (3.20) in the alternative form

$$L_0\Phi-2w^3\frac{\int f(w)\Phi}{\int w^3}=\lambda\Phi\,, \tag{4.8a}$$

where $L_0\Phi\equiv\Phi''-\Phi+3w^2\Phi$, and $f(w)$ is defined by

$$f(w)\equiv\frac{3}{2(1+\kappa_q)}w^2+\frac{(q+2)\kappa_q}{2(1+\kappa_q)}w^{q+1}\frac{\int w^3}{\int w^{q+2}}-\frac{q\kappa_q}{2(1+\kappa_q)}w^{q-1}\frac{\int w^3}{\int w^q}\,. \tag{4.8b}$$

When $\kappa_q=0$, where $f(w)=3w^2/2$, the NLEP (4.8a) has no unstable eigenvalues by Theorem 1 of [26] (see also Lemma 3.2 of [11]).

We multiply (4.8a) by the conjugate $\bar{\Phi}$ and integrate over the real line. Upon integrating by parts and taking the real part, we get

$$I_q[\Phi_R]+I_q[\Phi_I]=-\lambda_R\int|\Phi|^2\,, \tag{4.9}$$

where $\Phi=\Phi_R+i\Phi_I$ and $\lambda=\lambda_R+i\lambda_I$. Here the quadratic form is defined by

$$I_q[\Phi]\equiv\int\left(\left(\Phi'\right)^2+\Phi^2-3w^2\Phi^2\right)+2\frac{\int w^3\Phi\int f(w)\Phi}{\int w^3}\,. \tag{4.10}$$

To show that $\lambda_R<0$, so that there are no unstable eigenvalues of the NLEP (4.8), it is sufficient to show that the quadratic form $I_q[\Phi]$ is positive definite. In Appendix C, we establish the following lemma for $I_0[\Phi]$.

Lemma 4.1 *We have* $I_0[\Phi]>0\quad\forall\Phi\not\equiv 0$.

Since $I_0[\Phi]>0$, our strategy is to continue in $\kappa_q>0$ until we reach a point for which $I_q[\Phi]$ ceases to be positive definite. To analyse this transition, we observe that $I_q[\Phi]=\int-\Phi\mathcal{L}\Phi$,

https://doi.org/10.1017/S0956792519000305 Published online by Cambridge University Press

where $\mathcal{L}\Phi$ is the linear operator

$$\mathcal{L}\Phi \equiv L_0\Phi - \frac{\int f(w)\Phi}{\int w^3} w^3 - \frac{\int w^3\Phi}{\int w^3} f(w)\,. \tag{4.11}$$

Since $\mathcal{L}$ is self-adjoint, it follows that $I_q[\Phi]$ is positive definite if and only if $\mathcal{L}$ has only negative eigenvalues. This motivates the consideration of the following zero-eigenvalue problem for $\mathcal{L}$:

$$\mathcal{L}\Phi = 0\,, \qquad \Phi \in L^2(\mathbb{R})\,, \qquad \Phi \not\equiv 0\,. \tag{4.12}$$

To analyse (4.12), we use (4.11) to get

$$\Phi = \frac{\int f(w)\Phi}{\int w^3} L_0^{-1} w^3 + \frac{\int w^3\Phi}{\int w^3} L_0^{-1} f(w)\,. \tag{4.13}$$

Define $c_1 = \int f(w)\Phi$ and $c_2 = \int w^3\Phi$. By multiplying (4.13) by $f(w)$ and then by w^3, we get the linear system

$$c_1 = c_1 \frac{\int f(w) L_0^{-1} w^3}{\int w^3} + c_2 \frac{\int f(w) L_0^{-1} f(w)}{\int w^3}\,, \qquad c_2 = c_1 \frac{\int w^3 L_0^{-1} w^3}{\int w^3} + c_2 \frac{\int w^3 L_0^{-1} f(w)}{\int w^3}\,. \tag{4.14}$$

Upon using $L_0^{-1} w^3 = w/2$, and integrating by parts, we obtain that (4.14) has a nontrivial solution iff $g(\kappa_q) = 0$, where

$$g(\kappa_q) \equiv \det \begin{pmatrix} \frac{\int wf(w)}{2\int w^3} - 1 & \frac{\int f(w) L_0^{-1} f(w)}{\int w^3} \\ \frac{\int w^4}{2\int w^3} & \frac{\int wf(w)}{2\int w^3} - 1 \end{pmatrix} = \left(\frac{\int wf(w)}{2\int w^3} - 1 \right)^2 - \frac{\int w^4}{2\left(\int w^3\right)^2} \int f(w) L_0^{-1} f(w)\,. \tag{4.15}$$

When $\kappa_q = 0$, we have $f(w) = 3w^2/2$. Upon using $L_0^{-1} w^2 = w^2/3$, $\int w^4 = 16/3$ and $\int w^3 = \sqrt{2}\pi$, we calculate

$$g(0) = \frac{1}{16} - \frac{16}{3\pi^2} < 0\,. \tag{4.16}$$

Thus, when $\kappa_q = 0$, the only solution to (4.14) is $c_1 = c_2 = 0$, and so (4.11) becomes $L_0\Phi = 0$, which has no nontrivial even solution. By increasing κ_q, we conclude that a sufficient condition for guaranteeing no unstable eigenvalues of the NLEP (4.8) is that on the range $0 < \kappa_q < \kappa_{q0}$ we have $g(\kappa_q) < 0$. Here κ_{q0} is defined by

$$\kappa_{q0} = \sup\{\kappa_q \mid g(t) < 0\,,\ t \in (0, \kappa_q)\}\,. \tag{4.17}$$

In Figure 3, we plot $g(\kappa_q)$ vs. κ_q for $q = 2, 3, 4$. These results were obtained by numerically evaluating the integrals in (4.15), after computing $L_0^{-1} f(w)$ from a BVP solver. On the range for which $g(\kappa_q) < 0$, we conclude that $I_q[\Phi]$ is positive definite so that the NLEP (4.8) has no unstable eigenvalues.

As a partial confirmation of the results in Figure 3, we now show how to calculate $g(\kappa_q)$ analytically when $q = 2$. When $q = 2$, we have that $\psi \equiv L_0^{-1} f$ satisfies

$$L_0\psi = f\,, \qquad f = e_0 w^2 + e_1 w^3 + e_2 w\,, \tag{4.18a}$$

https://doi.org/10.1017/S0956792519000305 Published online by Cambridge University Press

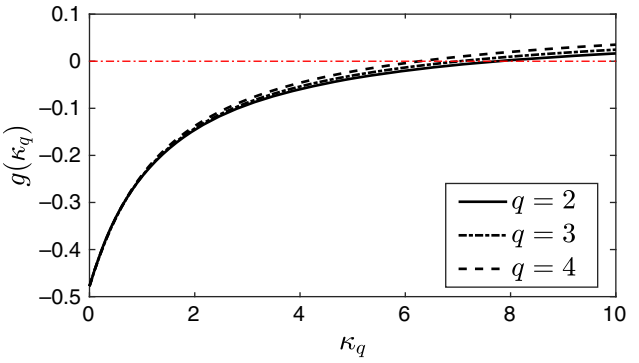

FIGURE 3. Plot of numerically computed $g(\kappa_q)$ vs. κ_q, as defined in (4.15), for $q = 2, 3, 4$. For $q = 2$, $g(\kappa_2)$ is given analytically in (4.22). On the range of κ_q for which $g(\kappa_q) < 0$, the NLEP (4.8) has no unstable eigenvalues.

where e_0, e_1 and e_2, are defined by

$$e_0 = \frac{3}{2(1+\kappa_2)}\,, \qquad e_1 = \frac{2\kappa_2}{1+\kappa_2}\frac{\int w^3}{\int w^4}\,, \qquad e_2 = -\frac{\kappa_2}{1+\kappa_2}\frac{\int w^3}{\int w^2}\,. \tag{4.18b}$$

Using (4.18a) for $f(w)$, we calculate

$$\frac{\int wf(w)}{2\int w^3} - 1 = \frac{3}{4(1+\kappa_2)} + \frac{\kappa_2}{2(1+\kappa_2)} - 1 = -\frac{(1+2\kappa_2)}{4(1+\kappa_2)}\,. \tag{4.19}$$

Next, upon using $L_0 w^2 = 3w^2$, $L_0 w = 2w^3$ and $L_0(w + yw') = 2w$, we calculate from (4.18a) that

$$\psi \equiv L_0^{-1} f = \frac{e_0}{3}w^2 + \frac{e_1}{2}w + \frac{e_2}{2}\left(w + yw'\right)\,. \tag{4.20}$$

Upon using (4.20) and (4.18b), we obtain after some rather lengthy, but straightforward, algebra that

$$\frac{\int w^4}{2\left(\int w^3\right)^2}\int f L_0^{-1} f = \frac{\kappa_2^2}{2(1+\kappa_2)^2} - \frac{1}{4(1+\kappa_2)^2}\left(\kappa_2^2 + 2\kappa_2\right)\frac{\int w^4}{\int w^2} + \frac{3}{8(1+\kappa_2)^2}\left(\frac{\int w^4}{\int w^3}\right)^2 + \frac{\kappa_2}{(1+\kappa_2)^2}\left[\frac{3}{4} + \frac{\int w^5}{2\int w^3}\right]\,. \tag{4.21}$$

We then simplify the expression in (4.21) using $\int w^4 = 16/3$, $\int w^2 = 4$, $\int w^3 = \sqrt{2}\pi$ and $\int w^5 = 3\sqrt{2}\pi/2$. In this way, and by combining the resulting expression with (4.19), we obtain from (4.15) that

$$g(\kappa_2) = \frac{1}{16(1+\kappa_2)^2}\left[(2\kappa_2+1)^2 - \frac{8}{3}\left(\kappa_2^2 + 5\kappa_2 + \frac{32}{\pi^2}\right)\right]\,. \tag{4.22}$$

Recalling the definition of the threshold κ_{20} in (4.17), a simple calculation using (4.22) yields $\kappa_{20} = \frac{1}{2}\left[7 + \sqrt{46 + 256/\pi^2}\right] \approx 7.74$. The formula for $g(\kappa_2)$ in (4.22), and the threshold κ_{20}, agrees with the numerical results shown in Figure 3.

In summary, we have shown that whenever $g(\kappa_q) < 0$ in (4.15), the NLEP (4.8) has no unstable eigenvalues. This sufficient condition for stability was implemented numerically for $q \neq 2$,

https://doi.org/10.1017/S0956792519000305 Published online by Cambridge University Press

and analytically for $q = 2$, which showed that the NLEP has no unstable eigenvalues for κ_q below some threshold. On the other hand, the numerical results in Figure 2 obtained from a finite difference approximation suggested that the NLEP (4.8) has no unstable eigenvalues *for all* $\kappa_q > 0$.

4.2.1 *No unstable eigenvalues for* $q = 2$ *and any* κ_2

In this subsection, we provide a different approach to prove that for $q = 2$ that there are no instabilities associated with synchronous perturbations of the hotspot amplitudes *for any* $\kappa_2 > 0$. For $q = 2$, this NLEP has the general form

$$L_0\Phi - w^3\left[a\int w^3\Phi + b\int w^2\Phi + c\int w\Phi\right] = \lambda\Phi\,, \quad \Phi \in L^2(\mathbb{R})\,; \quad L_0\Phi \equiv \Phi'' - \Phi + 3w^2\Phi\,. \tag{4.23}$$

We will convert this NLEP into one with a single nonlocal term proportional to $\int w\Phi$ using the two identities (cf. [22]):

$$L_0 w = 2w^3\,, \qquad L_0(w^2) = 3(w^2)\,. \tag{4.24}$$

Let Φ and λ be any eigenpair of (4.23). We first multiply (4.23) by w, and then use the first of (4.24), together with Green's identity, to obtain

$$\int wL_0\Phi = \int \Phi L_0 w = 2\int w^3\Phi = a\int w^4\int w^3\Phi + b\int w^4\int w^2\Phi + c\int w^4\int w\Phi + \lambda\int w\Phi\,. \tag{4.25a}$$

Next, we multiply (4.23) by w^2, and then use the second of (4.24), together with Green's identity, to obtain

$$\int w^2L_0\Phi = \int \Phi L_0 w^2 = 3\int w^2\Phi = a\int w^5\int w^3\Phi + b\int w^5\int w^2\Phi + c\int w^5\int w\Phi + \lambda\int w^2\Phi\,. \tag{4.25b}$$

Equations (4.25a) and (4.25b) provide a matrix system for $\int w^2\Phi$ and $\int w^3\Phi$ of the form

$$\begin{pmatrix} 3-\lambda-b\int w^5 & -a\int w^5 \\ b\int w^4 & a\int w^4 - 2 \end{pmatrix}\begin{pmatrix} \int w^2\Phi \\ \int w^3\Phi \end{pmatrix} = \begin{pmatrix} c\int w^5 \\ -\left(\lambda + c\int w^4\right) \end{pmatrix}\int w\Phi\,. \tag{4.26}$$

By inverting the matrix in (4.26), we obtain that

$$\begin{aligned} \int w^2\Phi &= \frac{-(2c+a\lambda)\int w^5}{(3-\lambda)\left(a\int w^4 - 2\right) + 2b\int w^5}\int w\Phi\,, \\ \int w^3\Phi &= \frac{-\left(\lambda + c\int w^4\right)(3-\lambda) + b\lambda\int w^5}{(3-\lambda)\left(a\int w^4 - 2\right) + 2b\int w^5}\int w\Phi\,, \end{aligned} \tag{4.27}$$

provided that

$$(3-\lambda)\left(a\int w^4 - 2\right) + 2b\int w^5 \neq 0\,. \tag{4.28}$$

https://doi.org/10.1017/S0956792519000305 Published online by Cambridge University Press

By substituting (4.27) into (4.23), and using $\int w^2 = 4$, we obtain after some algebra the following NLEP with a single nonlocal term:

$$L_0\Phi - 2w^3\gamma\frac{\int w\Phi}{\int w^2} = \lambda\Phi\,, \qquad \text{where} \qquad \gamma = \frac{2(3-\lambda)(a\lambda+2c)}{(\lambda-3)\left(a\int w^4 - 2\right) - 2b\int w^5}\,. \tag{4.29}$$

Conversely, suppose that Φ and λ be any eigenpair of (4.29). Upon multiplying (4.29) by w, and then by w^2, and using (4.24), we obtain from (4.29) that

$$(3-\lambda)\int w^2\Phi = 2\gamma\frac{\int w^5}{\int w^2}\int w\Phi\,, \qquad 2\int w^3\Phi = \left(2\gamma\frac{\int w^4}{\int w^2} + \lambda\right)\int w\Phi\,. \tag{4.30}$$

Next, by adding and subtracting terms in (4.29), we get

$$\begin{aligned} L_0\Phi - w^3\left[a\int w^3\Phi + b\int w^2\Phi + c\int w\Phi + \xi\right] &= \lambda\Phi\,,\\ \xi \equiv \left(\frac{2\gamma}{\int w^2} - c\right)\int w\Phi - b\int w^2\Phi - a\int w^3\Phi\,, & \end{aligned} \tag{4.31}$$

which reduces to (4.23) only when $\xi = 0$. We solve (4.30) for $\int w^3\Phi$, and for $\int w^2\Phi$ which requires $\lambda \neq 3$. Then, upon using (4.29) for γ, we can readily verify from (4.31) that $\xi = 0$. Therefore, any eigenpair of (4.29) with $\lambda \neq 3$ is also an eigenpair of (4.23).

For $q = 2$, the coefficients a, b and c in (4.2) associated with synchronous perturbations of the hotspot amplitudes are

$$a = \frac{4\kappa}{(1+\kappa)\int w^4}\,, \qquad b = \frac{3}{(1+\kappa)\int w^3}\,, \qquad c = -\frac{2\kappa}{(1+\kappa)\int w^2}\,, \tag{4.32}$$

where we label $\kappa \equiv \kappa_2$. By combining (4.32) and (4.29), and using $\int w^4/\int w^2 = 4/3$ and $\int w^5/\int w^3 = 3/2$, we get

$$\gamma = \frac{\kappa(3-\lambda)(3\lambda-4)}{2\left[2(\lambda-3)(\kappa-1)-9\right]}\,, \tag{4.33}$$

while the condition (4.28) becomes $(\lambda-3)(\kappa-1) \neq 9/2$.

To prove that (4.29), with γ as in (4.33), has no unstable eigenvalues we will use a key inequality that can readily be derived by proceeding as in (2.22) of [27] (see also equation (2.27) in Section 2 of [25]). Suppose that (4.29) has an eigenvalue with $\mathrm{Re}(\lambda) \geq 0$. Then, the following inequality must hold

$$\mathcal{T} \equiv 2\left(\frac{\int w^4}{\int w^2}\right)|\gamma-1|^2 + \mathrm{Re}\left[\bar{\lambda}(\gamma-1)\right] \leq 0\,, \tag{4.34}$$

where the bars denote modulus. From (4.33), we calculate that

$$\gamma - 1 = \frac{-3\lambda^2\kappa + \lambda(9\kappa+4) + 6}{4(\kappa-1)\lambda - 12\kappa - 6}\,. \tag{4.35}$$

We will now use (4.34), with (4.35), to show that the NLEP (4.29) cannot have any purely imaginary eigenvalues of the form $\lambda = i\omega$. For $\lambda = i\omega$, we write $\gamma - 1$ in (4.35) as

$$\gamma - 1 = \frac{z_1}{z_2}\,, \qquad z_1 = 6 + 3\omega^2\kappa + i\omega(9\kappa+4)\,, \qquad z_2 = -6(1+2\kappa) + 4i\omega(\kappa-1)\,. \tag{4.36}$$

https://doi.org/10.1017/S0956792519000305 Published online by Cambridge University Press

Using $\int w^4 / \int w^2 = 4/3$, we calculate from (4.34) that

$$\mathcal{T} = \frac{8}{3}\frac{|z_1|^2}{|z_2|^2} + \mathrm{Re}\left(-i\omega\frac{z_1}{z_2}\right) = \frac{8}{3}\frac{|z_1|^2}{|z_2|^2} - \mathrm{Re}\left(\frac{i\omega z_1\bar{z}_2}{|z_2|^2}\right) = \frac{1}{3|z_2|^2}\left[8|z_1|^2 + 3\omega\mathrm{Im}\,(z_1\bar{z}_2)\right]. \tag{4.37}$$

Upon substituting (4.36) into (4.37), we obtain after some rather lengthy, but straightforward, algebra that

$$\mathcal{T} = \frac{12}{36(1+2\kappa)^2 + 16\omega^2(\kappa-1)^2}\left[\kappa(\kappa+1)\omega^4 + \frac{\omega^2}{18}\left(162\kappa^2 + 243\kappa + 64\right) + 8\right]. \tag{4.38}$$

This shows that $\mathcal{T} > 0$ holds $\forall \kappa > 0$ and ω. From our key inequality (4.34), it follows that the NLEP (4.29) does not undergo a Hopf bifurcation for any $\kappa \geq 0$.

To conclude the analysis of linear stability, we use a continuation argument in κ. With a, b and c as given in (4.32), the NLEP (4.23) has no unstable eigenvalues when $\kappa = 0$ by Theorem 1 of [26] (see also Lemma 3.2 of [11]). By our established correspondence between the two NLEPs (4.23) and (4.29), this linear stability result can also be seen from (4.29), as (4.29) has no unstable eigenvalues with $\lambda \neq 3$ when $\kappa = 0$. This latter result is immediate since when $\kappa = 0$, we have $\gamma = 0$ in (4.29). Therefore, (4.29) reduces to $L_0\Phi = \lambda\Phi$, which has no unstable eigenvalues with $\lambda \neq 3$ (cf. [7]).

Next, if we continue in κ, we claim that all eigenvalues of (4.23) must remain in the stable left half-plane $\mathrm{Re}(\lambda) \leq 0$. We establish this by contradiction. Suppose that at some point $\kappa = \kappa_0 > 0$, a branch $\lambda = \lambda(\kappa)$ of eigenvalues crosses the imaginary axis, i.e. it satisfies $\mathrm{Re}(\lambda) = 0$ and $\frac{d}{d\kappa}\mathrm{Re}(\lambda) > 0$ for some $\kappa = \kappa_0$. Since $\lambda(\kappa_0)$ is pure imaginary, it follows that $(\lambda - 3)(\kappa - 1) \neq 9/2$, and so the restriction (4.28) holds. Therefore, this eigenvalue must satisfy the NLEP (4.29) with only one nonlocal term. Our proof above that the NLEP (4.29) has no purely imaginary eigenvalue provides the required contradiction.

The key qualitative conclusion from this $q = 2$ 'cops-on-the-dots' analysis is that for $\mathcal{O}(1) \ll D_p \ll \mathcal{O}(\epsilon^{-3})$ (see (3.8)), there can be no synchronous linear instabilities of the amplitudes of a multi-hotspot steady state for any policing level U_0 below the threshold $U_{0,\max}$ for which steady-state hotspot solutions exist.

5 Analysis of the NLEP: Competition instability

In this section, we will analyse zero-eigenvalue crossings for the NLEP (3.22), corresponding to asynchronous perturbations of the hotspot amplitudes. This zero-eigenvalue crossing will yield $K - 1$ critical values of the criminal diffusivity $\mathcal{D}$. We will determine the behaviour of this stability threshold in terms of the police focus parameter q and policing level U_0.

To determine the zero-eigenvalue crossing, we observe from (3.22) that when $\lambda = 0$, we have that $L_0\Phi$ is proportional to w^3. As a result, by recalling the identity $L_0 w = 2w^3$, and noting that $\chi_2 = 0$ when $\lambda = 0$, it follows that (3.22) has a zero eigenvalue, with corresponding eigenfunction $\Phi = w$, when

$$2 = 3\chi_0 + (q+2)\chi_1. \tag{5.1}$$

https://doi.org/10.1017/S0956792519000305 Published online by Cambridge University Press

Using (3.22b) for χ_0 and χ_1, we solve (5.1) for $\mathcal{D}_u$ to conclude that the NLEP (3.22) has a zero eigenvalue at the critical value of $\mathcal{D}_u$ given by

$$\mathcal{D}_u = \frac{1}{2}\left(1 + q\kappa_q\right), \qquad \text{where} \qquad \kappa_q = \frac{2q}{q+1}\frac{U_0}{\omega}\,. \tag{5.2}$$

Then, using (3.23), it follows that a zero-eigenvalue crossing occurs at $\mathcal{D} = \mathcal{D}_j$, for $j = 1, \ldots, K-1$, given by

$$\mathcal{D}_j = \frac{S}{8K^4\pi^2\alpha^2\left[1-\cos\left(\frac{\pi j}{K}\right)\right]}\left[\omega^3 + \frac{2q^2U_0}{q+1}\omega^2\right], \qquad j = 1, \ldots, K-1\,. \tag{5.3}$$

The smallest such threshold $\mathcal{D}_c = \min_j \mathcal{D}_j$ on $j = 1, \ldots, K-1$, referred to as the competition stability threshold, occurs when $j = K-1$. We write $\mathcal{D}_c$ as

$$\mathcal{D}_c \equiv \mathcal{D}_{K-1} = \frac{S}{8K^4\pi^2\alpha^2\left[1+\cos\left(\pi/K\right)\right]}g(U_0;q)\,, \tag{5.4a}$$

where $g(U_0;q)$ is defined on the range $0 \le U_0 < U_{0,\max} = S(\gamma-\alpha)(q+1)/(2q)$ by

$$g(U_0;q) \equiv \omega^3 + \left(\frac{2q^2}{q+1}U_0\right)\omega^2 = (1-q)\omega^3 + qS(\gamma-\alpha)\omega^2\,, \qquad \text{where} \qquad \omega = S(\gamma-\alpha) - 2qU_0/(q+1)\,. \tag{5.4b}$$

For a general value of $q > 1$, owing to the presence of the three distinct nonlocal terms in (3.22), it is analytically intractable to perform a full linear stability analysis of hotspot steady states on either side of the zero-eigenvalue crossing value $\mathcal{D} = \mathcal{D}_c$. For the specific $q = 2$ 'cops-on-the-dots' case, where some key identities can be used to reduce (3.22) to an NLEP with only one nonlocal term, this linear stability problem is studied in Section 6 using a hybrid analytical–numerical approach. However, for a general $q > 1$, in Section 5.1 we show analytically that the NLEP (3.22) always has a unique unstable eigenvalue in $\mathrm{Re}(\lambda) > 0$ whenever $\mathcal{D} > \mathcal{D}_c$ and $\tau_u \to 0^+$, and has no unstable eigenvalue when $\mathcal{D} < \mathcal{D}_c$. In view of (3.24) relating D_p to τ_u and the range (3.8) of D_p, this partial result proves that when $\mathcal{O}(\epsilon^{1-q}) \ll D_p \ll \mathcal{O}(\epsilon^{-1-q})$, the hotspot steady state constructed for $q > 1$ is always unstable when $\mathcal{D}$ exceeds $\mathcal{D}_c$.

In the remainder of this subsection, we examine how the competition stability threshold $\mathcal{D}_c$ depends on the degree q of patrol focus and the level U_0 of police deployment. From (2.12), the maximum $A_{\max}$ of the steady-state attractiveness field is $A_{\max} \sim \epsilon^{-1}\omega/(K\pi)$, which decreases as either ω decreases or as K increases. From Corollary 2.2, we observe that the criminal density ρ at the hotspot locations is $\rho_{\max} = [w(0)]^2 = 2$, which is independent of q and U_0, with $\rho = \mathcal{O}(\epsilon^2)$ away from the hotspot regions. As a result, the total crime is reduced primarily by decreasing the number of stable steady-state hotspots on the given domain. As such, we seek to tune the police parameters q and U_0 so that the range of diffusivity $\mathcal{D}$ for which a K-hotspot steady state is unstable when $\tau_u \to 0^+$ (see Section 5.1 below) is as large as possible. This corresponds to minimising the competition stability threshold $\mathcal{D}_c$ in (5.4), which is determined in terms of $g(U_0;q)$ in (5.4b).

https://doi.org/10.1017/S0956792519000305 Published online by Cambridge University Press

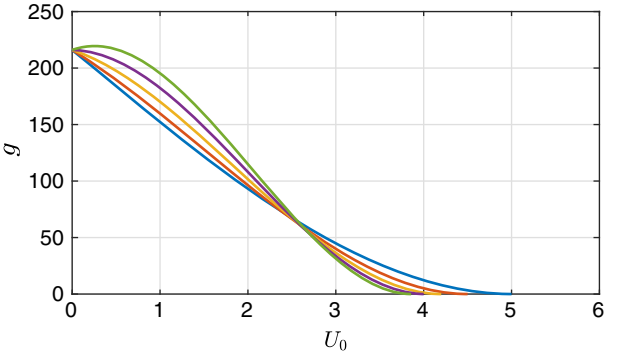

FIGURE 4. Competition stability threshold nonlinearity $g(U_0; q)$, as defined in (5.4b), vs. U_0 on the range $0 < U_0 < U_{0,\max} \equiv S(\gamma - \alpha)(q+1)/(2q)$ for $q = 1.5, 2.0, 2.5, 3.0, 3.5$, when $S = 6$, $\gamma = 2$ and $\alpha = 1$. Smaller values of q correspond to larger values of $U_{0,\max}$, as represented by the intercept on the horizontal U_0 axis.. Notice that g is not monotone in U_0 when $q > 3$. From (5.4), the competition threshold $\mathcal{D}_c$ is a positive scaling of $g(U_0; q)$.

We first fix $q > 1$ and study how $g(U_0; q)$ depends on U_0. On $0 < U_0 < U_{0,\max} \equiv S(\gamma - \alpha)(q+1)/(2q)$, we find that

$$\frac{dg}{dU_0} = -\omega \frac{2q}{q+1}\left[\frac{6q(q-1)}{q+1}U_0 + (3-q)S(\gamma-\alpha)\right]. \tag{5.5}$$

This shows that $dg/dU_0 < 0$ on $0 < U_0 < U_{0,\max}$ whenever $1 < q < 3$. Thus, when the patrol is not too focused, i.e. when $1 < q < 3$, increasing the overall policing level leads to a larger range of $\mathcal{D}$ where the hotspot steady state is unstable when $\tau_u \to 0^+$. For $q > 3$, (5.5) also yields that

$$\begin{aligned} &\frac{dg}{dU_0} > 0 \quad \text{on} \quad 0 < U_0 < S(\gamma-\alpha)\left(\frac{q-3}{3(q-1)}\right) < U_{0,\max}; \\ &\frac{dg}{dU_0} < 0 \quad \text{on} \quad S(\gamma-\alpha)\left(\frac{q-3}{3(q-1)}\right) < U_0 < U_{0,\max}. \end{aligned} \tag{5.6}$$

Therefore, with an overly focused police patrol (i.e. $q > 3$), the hotspot steady state is destabilised only by having a sufficiently large policing level. This is illustrated in Figure 4 where we plot $g(U_0; q)$ vs. U_0 for several values of q.

Next, we fix U_0 in $0 < U_0 < U_{0,\max}$ and determine how $g(U_0; q)$ depends on q for $q > 1$. We readily calculate that

$$\frac{dg}{dq} = \frac{2\omega U_0}{(q+1)^3}\left[\omega(q+3)(q^2-1) - 4q^2U_0\right], \qquad \text{where} \qquad \omega \equiv S(\gamma-\alpha) - 2qU_0/(q+1). \tag{5.7}$$

This shows that $dg/dq < 0$ if $0 < \omega < 4q^2U_0/[(q+3)(q^2-1)]$. Using (5.7) for ω in terms of U_0, this inequality yields

$$\frac{dg}{dq} < 0 \quad \text{when} \quad U_{0,\max}\left[1 + \frac{2q}{(q+3)(q-1)}\right]^{-1} < U_0 < U_{0,\max}. \tag{5.8}$$

The qualitative interpretation of this result is that if the policing level is sufficiently close to its maximum value $U_{0,\max}$, an increase in the patrol focus parameter q yields a larger range in $\mathcal{D}$

https://doi.org/10.1017/S0956792519000305 Published online by Cambridge University Press

where the hotspot steady state is unstable when $\tau_u \to 0^+$, or equivalently when $\mathcal{O}(\epsilon^{1-q}) \ll D_p \ll \mathcal{O}(\epsilon^{-1-q})$.

5.1 Large police diffusivity $\mathcal{O}(\epsilon^{1-q}) \ll D_p \ll \mathcal{O}(\epsilon^{-1-q})$: An instability result for $\mathcal{D} > \mathcal{D}_c$

Letting $\tau_u \to 0^+$, corresponding to the parameter range $\mathcal{O}(\epsilon^{1-q}) \ll D_p \ll \mathcal{O}(\epsilon^{-1-q})$, we now prove that the NLEP (3.22), which applies to asynchronous perturbations of the amplitudes of the steady-state hotspot pattern, has an unstable positive real eigenvalue whenever $\mathcal{D}_u > \frac{1}{2}\left(1 + q\kappa_q\right)$. This will establish that a multi-hotspot steady state is unstable for this range of D_p whenever $\mathcal{D}$ exceeds the competition stability threshold $\mathcal{D}_c$ defined in (5.4). When $\tau_u \to 0^+$, we have $\chi_2 = 0$ and so (3.22) reduces to an NLEP with two nonlocal terms

$$L_0\Phi - \chi_0 w^3\left(3\frac{\int w^2\Phi}{\int w^3}\right) - \chi_1 w^3\left((q+2)\frac{\int w^{q+1}\Phi}{\int w^{q+2}}\right) = \lambda\Phi\,, \qquad \text{where } \chi_0 = \frac{1}{\left(1+\kappa_q+\mathcal{D}_u\right)}\,, \quad \chi_1 = \chi_0\kappa_q\,. \tag{5.9}$$

To analyse (5.9), we first reformulate it into an NLEP with only one nonlocal term using the key identity $L_0(w^2) = 3(w^2)$ (cf. [22]). Upon multiplying (5.9) by w^2, and then using Green's identity, we readily calculate that

$$\int w^2\Phi\left(3 - 3\chi_0\frac{\int w^5}{\int w^3} - \lambda\right) = \chi_1(q+2)\left(\frac{\int w^5}{\int w^{q+2}}\right)\int w^{q+1}\Phi\,. \tag{5.10}$$

Since $\int w^5/\int w^3 = 3/2$ from (2.5), (5.10) yields that

$$\int w^2\Phi = \left(\frac{\chi_1(q+2)\int w^5}{3 - \frac{9\chi_0}{2} - \lambda}\right)\frac{\int w^{q+1}\Phi}{\int w^{q+2}}\,, \tag{5.11}$$

provided that $\lambda \neq 3 - 9\chi_0/2$. Then, by substituting (5.11) back into (5.9), and using $\chi_1 = \chi_0\kappa_q$, we obtain the following equivalent NLEP with only one nonlocal term (provided that $\lambda \neq 3 - 9\chi_0/2$):

$$L_0\Phi - \chi_c(\lambda)w^3\frac{\int w^{q+1}\Phi}{\int w^{q+2}} = \lambda\Phi\,, \qquad \text{where} \qquad \chi_c(\lambda) \equiv \chi_0\kappa_q(q+2)\left(\frac{3-\lambda}{3 - \frac{9\chi_0}{2} - \lambda}\right)\,. \tag{5.12}$$

To interpret the apparent restriction that $\lambda \neq 3 - 9\chi_0/2$, we observe that since $\chi_1 = \chi_0\kappa_q$ is proportional to U_0 (see (3.22b) for the definition of κ_q), it follows from (5.10) that for any eigenpair for which $\int w^{q+1}\Phi \neq 0$ for any $q > 1$, we must have $\lambda = 3 - 9\chi_{0,j}/2$ if and only if $U_0 = 0$. For the case of no police, this recovers the result in equation (3.17) of [11] for the unique discrete eigenvalue of the linearisation of a K-hotspot steady state of the basic two-component crime model.

We now show that the reformulated NLEP (5.12) has an unstable real eigenvalue whenever $\mathcal{D}_u > \frac{1}{2}\left(1 + q\kappa_q\right)$. To do so, we convert (5.12) into a root-finding problem. We write $\Phi = \chi_c\left(L_0 - \lambda\right)^{-1} w^3\int w^{q+1}\Phi/\int w^{q+2}$, multiply both sides by w^{q+1}, and then integrate over the real line. In this way, and using (5.9) for χ_0, we readily find that any discrete eigenvalue of (5.12) in $\mathrm{Re}(\lambda) > 0$ must be a root of $\zeta(\lambda) = 0$ defined by

$$\zeta(\lambda) \equiv \mathcal{C}_c(\lambda) - \mathcal{F}(\lambda)\,, \tag{5.13a}$$

https://doi.org/10.1017/S0956792519000305 Published online by Cambridge University Press

where

$$\mathcal{C}_c(\lambda) \equiv \frac{1}{\chi_c(\lambda)} = \frac{\left(1+\kappa_q+\mathcal{D}_u\right)}{\kappa_q(q+2)} + \frac{9}{2\kappa_q(q+2)(\lambda-3)}, \quad \text{and} \quad \mathcal{F}(\lambda) \equiv \frac{\int w^{q+1}\,(L_0-\lambda)^{-1}\,w^3}{\int w^{q+2}}. \tag{5.13b}$$

When $\mathcal{D}_u > \frac{1}{2}\left(1+q\kappa_q\right)$, we claim that $\zeta(\lambda)=0$ has a real root in $0<\lambda<3$, which yields an unstable eigenvalue for the NLEP (5.12). To show this, we use $L_0 w = 2w^3$ to calculate $\mathcal{F}(0) = \int w^{q+1} L_0^{-1}(w^3)/\int w^{q+2} = 1/2$, and observe that $\mathcal{F}(\lambda)\to+\infty$ as $\lambda\to\nu_0^-$, where $\nu_0=3$ is the unique positive eigenvalue of L_0 (cf. [7, 22]). Moreover, we observe that

$$\mathcal{C}_c(\lambda)\to-\infty \quad \text{as} \quad \lambda\to 3^-, \qquad \text{and} \qquad \mathcal{C}_c(0) = \frac{\left(\kappa_q+\mathcal{D}_u-1/2\right)}{\kappa_q(q+2)},$$

which yields that $\mathcal{C}_c(0)>1/2$ when $\mathcal{D}_u > \frac{1}{2}\left(1+q\kappa_q\right)$. With these properties of $\mathcal{C}_c(\lambda)$ and $\mathcal{F}(\lambda)$, it follows from the intermediate value theorem that $\zeta(\lambda)$ has a root at some value of λ on $0<\lambda<3$.

This simple result proves that a multi-hotspot steady state is unstable for $\tau_u\to 0^+$, or equivalently for D_p on the range $\mathcal{O}(\epsilon^{1-q}) \ll D_p \ll \mathcal{O}(\epsilon^{-1-q})$ whenever $\mathcal{D}$ exceeds the competition stability threshold $\mathcal{D}_c$ in (5.4).

Next, using a winding number criterion, we now obtain a more precise result for the spectrum of the NLEP (5.12), which pertains to the special case $\tau_u\to 0^+$. We do so by determining the number N of zeroes of $\zeta(\lambda)$ in $\mathrm{Re}(\lambda)>0$, which corresponds to the number (counting multiplicity) of unstable eigenvalues of the NLEP (5.12).

To determine N, we calculate the winding of $\zeta(\lambda)$ over the Nyquist contour Γ traversed in the counterclockwise direction that consists of the positive and negative imaginary axis, defined by Γ_I^+ $(0<\mathrm{Im}(\lambda)<iR,\ \mathrm{Re}(\lambda)=0)$ and Γ_I^- $(-iR<\mathrm{Im}(\lambda)<0,\ \mathrm{Re}(\lambda)=0)$, respectively, together with the semi-circle C_R defined by $|\lambda|=R>0$ for $|\arg(\lambda)|<\pi/2$. From (5.13b), $\mathcal{C}_c(\lambda)$ is a meromorphic function with a simple pole at $\lambda=3$, whereas $\mathcal{F}(\lambda)$ is analytic in $\mathrm{Re}(\lambda)\geq 0$ except at the simple pole at $\lambda=3$. The simple poles of $\mathcal{C}(\lambda)$ and $\mathcal{F}(\lambda)$ do not cancel as $\lambda\to 3^-$, since when restricted to the real line we have $\mathcal{F}(\lambda)\to+\infty$ while $\mathcal{C}(\lambda)\to-\infty$ as $\lambda\to 3^-$. Therefore, $\zeta(\lambda)=\mathcal{C}(\lambda)-\mathcal{F}(\lambda)$ has a simple pole at $\lambda=3$. Then, since $\zeta(\lambda)$ is bounded on C_R as $R\to\infty$, and $\zeta(\bar{\lambda})=\overline{\zeta(\lambda)}$, we let $R\to\infty$ and obtain from the argument principle that

$$N = 1 + \frac{1}{\pi}\left[\arg\zeta\right]_{\Gamma_I^+}. \tag{5.14}$$

Here $[\arg\zeta]_{\Gamma_I^+}$ denotes the change in the argument of ζ as $\lambda=i\lambda_I$ is traversed down the positive imaginary axis $0<\lambda_I<\infty$.

To calculate this argument change, we let $\lambda=i\lambda_I$ and decompose $\zeta(i\lambda_I)=\zeta_R(\lambda_I)+i\zeta_I(\lambda_I)$ and $\mathcal{F}(i\lambda_I)=\mathcal{F}_R(\lambda_I)+i\mathcal{F}_I(\lambda_I)$, to obtain from (5.13) that

$$\mathrm{Im}\left[\zeta(i\lambda_I)\right] \equiv \zeta_I(\lambda_I) = -\frac{b\lambda_I}{9+\lambda_I^2} - \mathcal{F}_I(\lambda_I), \tag{5.15a}$$

where $b\equiv 9\left[2\kappa_q(q+2)\right]^{-1}$ and $\mathcal{F}_I(\lambda_I)\equiv\mathrm{Im}\left[\mathcal{F}(i\lambda_I)\right]$ is given by

$$\mathcal{F}_I(\lambda_I) = \frac{\lambda_I\int w^{q+1}\left[L_0^2+\lambda_I^2\right]^{-1}w^3}{\int w^{q+2}}. \tag{5.15b}$$

https://doi.org/10.1017/S0956792519000305 Published online by Cambridge University Press

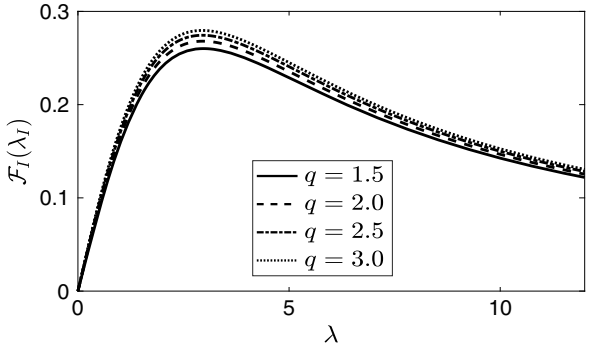

FIGURE 5. Plot of $\mathcal{F}_I(\lambda_I)$ vs. λ_I, defined in (5.15b), for $q = 1.5, 2.0, 2.5, 3.0$ on the range $0 < \lambda_I < 12$. This function is rather insensitive to changes in q.

Proposition 4.3 of [22] established that $\mathcal{F}_I(\lambda_I) > 0$ on $\lambda_I > 0$ when $q = 2$. Based on the numerical evidence shown in Figure 5, for both integer and non-integer values of q, we make the following conjecture:

Conjecture 5.1 *Consider $\mathcal{F}_I(\lambda_I) \equiv Im\,[\mathcal{F}(i\lambda_I)]$ as defined by (5.15b). Then, $\mathcal{F}_I(\lambda_I) > 0$ on $\lambda_I > 0$ holds for all $q > 1$.*

Assuming that this conjecture holds, we obtain the key inequality from (5.15a) that $\mathrm{Im}\,[\zeta(i\lambda_I)] < 0$ for all $\lambda_I > 0$. Next, we observe that as $\lambda_I \to \infty$ we have $\zeta(i\lambda_I) \to \left(1 + \kappa_q + \mathcal{D}_u\right)/[\kappa_q(q+2)] > 0$, and that $\zeta(0) = \mathcal{C}_c(0) - 1/2$ satisfies

$$\zeta(0) > 0 \quad \text{if} \quad \mathcal{D}_u > \frac{1}{2}\left(1 + q\kappa_q\right) ; \qquad \zeta(0) < 0 \quad \text{if} \quad \mathcal{D}_u < \frac{1}{2}\left(1 + q\kappa_q\right) . \tag{5.16}$$

We readily conclude from these results that $[\arg\zeta]_{\Gamma_I^+} = 0$ when $\mathcal{D}_u > \frac{1}{2}\left(1 + q\kappa_q\right)$ and $[\arg\zeta]_{\Gamma_I^+} = -\pi$ when $\mathcal{D}_u < \frac{1}{2}\left(1 + q\kappa_q\right)$. From (5.14), it follows that $N = 1$ when $\mathcal{D}_u > \frac{1}{2}\left(1 + q\kappa_q\right)$ and that $N = 0$ otherwise. We summarise our result as follows:

Proposition 5.2 *Let $\tau_u \to 0^+$, which corresponds to the range $\mathcal{O}(\epsilon^{1-q}) \ll D_p \ll \mathcal{O}(\epsilon^{-1-q})$ of police diffusivity. Assume that Conjecture 5.1 holds for $q > 1$. Then, under the conditions of Proposition 3.4, a multi-hotspot steady-state solution is unstable to asynchronous perturbations of the hotspot amplitudes for an arbitrary $q > 1$ when $\mathcal{D} > \mathcal{D}_c$, and is linearly stable to such perturbations whenever $\mathcal{D} < \mathcal{D}_c$. The instability when $\mathcal{D} > \mathcal{D}_c$ is due to a unique unstable eigenvalue in the spectrum of the NLEP (5.12). Here $\mathcal{D}_c$ is the competition threshold defined in (5.4).*

This result provides a necessary and sufficient condition for the linear stability of the multi-hotspot steady state for an arbitrary $q > 1$. In the next section, we determine more refined stability results for the special case $q = 2$ corresponding to 'cops-on-the-dots'.

6 Asynchronous perturbations: Linear stability analysis for $q = 2$

In this section, we analyse the spectrum of the NLEP (3.22), relevant to asynchronous perturbations of the hotspot amplitudes, for the specific case of cops-on-the-dots where $q = 2$. For $q = 2$,

https://doi.org/10.1017/S0956792519000305 Published online by Cambridge University Press

in Section 6.1, we reformulate the NLEP (3.22) with three nonlocal terms into an NLEP with a single nonlocal term proportional to $\int w^3\Phi$, which is then more readily analysed. We will show that a police diffusivity on the range $D_p = \mathcal{O}(\epsilon^{-1})$ leads to the possibility of oscillatory instabilities of the hotspot amplitudes when $\mathcal{D}$ is below the competition stability threshold.

6.1 Reformulation as an NLEP with one nonlocal term

For $q = 2$, the NLEP (3.22) for $\Phi \in L^2(\mathbb{R})$ has the form given in (4.23), where a, b and c are now defined by

$$a \equiv \frac{4\chi_1}{\int w^4}\,, \qquad b \equiv \frac{3\chi_0}{\int w^3}\,, \qquad c \equiv \frac{2\chi_2}{\int w^2}\,, \tag{6.1}$$

in terms of χ_0, χ_1 and χ_2 as given in (3.22b).

We will convert the NLEP (4.23) with three nonlocal terms into an NLEP with a single nonlocal term proportional to $\int w^3\Phi$, instead of proportional to $\int w\Phi$ as in (4.29) of Section 4.2.1. This alternative reduction is needed for the study of asynchronous perturbations since from (3.22b) we have that χ_2, and thus c, vanishes linearly in λ as $\lambda \to 0$. With such a vanishing c, we would have that γ^{-1} in (4.29) is not analytic at $\lambda = 0$, which makes (4.29) problematic for analysis. As such, we require a different reformulation.

Let Φ and λ be any eigenpair of (4.23) with a, b and c as defined in (6.1), in which $\lim_{\lambda\to 0}\lambda^{-1}c = c_0$ where c_0 is finite and non-zero. Then, proceeding as in the derivation of (4.25a) and (4.25b), we obtain the matrix system

$$\begin{pmatrix} b\int w^4 & c\int w^4 + \lambda \\ 3 - \lambda - b\int w^5 & -c\int w^5 \end{pmatrix}\begin{pmatrix} \int w^2\Phi \\ \int w\Phi \end{pmatrix} = \begin{pmatrix} 2 - a\int w^4 \\ a\int w^5 \end{pmatrix}\int w^3\Phi\,. \tag{6.2}$$

By inverting the matrix in (6.2), we calculate that

$$\begin{aligned} \int w^2\Phi &= \frac{-(2c + a\lambda)\int w^5}{b\lambda\int w^5 - \left(c\int w^4 + \lambda\right)(3-\lambda)}\int w^3\Phi\,, \\ \int w\Phi &= \frac{(\lambda - 3)(2 - a\int w^4) + 2b\int w^5}{b\lambda\int w^5 - \left(c\int w^4 + \lambda\right)(3-\lambda)}\int w^3\Phi\,, \end{aligned} \tag{6.3}$$

provided that

$$b\lambda\int w^5 - \left(c\int w^4 + \lambda\right)(3-\lambda) \neq 0\,. \tag{6.4}$$

By substituting (6.3) into (4.23), we obtain after some algebra, the following NLEP with a single nonlocal term:

$$L_0\Phi - \chi w^3\frac{\int w^3\Phi}{\int w^4} = \lambda\Phi\,, \qquad \text{where} \qquad \chi = \frac{(\lambda-3)(2c + a\lambda)\int w^4}{b\lambda\int w^5 - \left(c\int w^4 + \lambda\right)(3-\lambda)}\,. \tag{6.5}$$

Remark 6.1 *The multiplier χ in the NLEP (6.5) is well defined at $\lambda = 0$ when $\lim_{\lambda\to 0} c/\lambda = c_0$ with c_0 finite and non-zero. This case is relevant to the study of the linear stability of asynchronous perturbations of the hotspot amplitudes.*

https://doi.org/10.1017/S0956792519000305 Published online by Cambridge University Press

We have so far established that, provided the condition (6.4) holds, an eigenpair of (4.23) is also an eigenpair of (6.5). To complete the equivalence between (4.23) and (6.5), we now suppose that Φ, λ is an eigenpair of (6.5). Upon multiplying (6.5) by w, and then by w^2, we use the identities (4.24) to readily derive that

$$(2-\chi)\int w^3\Phi = \lambda\int w\Phi\,, \qquad (3-\lambda)\int w^2\Phi = \chi\frac{\int w^5}{\int w^4}\int w^3\Phi\,. \tag{6.6}$$

We then add and subtract in (6.5) to get

$$\begin{aligned} L_0\Phi - w^3\left[a\int w^3\Phi + b\int w^2\Phi + c\int w\Phi + \xi\right] &= \lambda\Phi\,,\\ \xi \equiv \left(\frac{\chi}{\int w^4} - a\right)\int w^3\Phi - b\int w^2\Phi - c\int w\Phi\,, & \end{aligned} \tag{6.7}$$

which reduces to (4.23) only when $\xi = 0$. We calculate using (6.6) that for $\lambda \neq 3$, and $\lim_{\lambda\to 0} c/\lambda$ finite and non-zero, that

$$\xi = \left(\frac{\chi}{\int w^4} - a - \frac{b\chi}{3-\lambda}\frac{\int w^5}{\int w^4} - \frac{c(2-\chi)}{\lambda}\right)\int w^3\Phi\,. \tag{6.8}$$

Finally, using (6.5) for χ in (6.8), we get $\xi = 0$, so that (6.7) reduces to (4.23).

The relationship between the spectra of (4.23) and of (6.5) is summarised as follows:

Lemma 6.2 *Let Φ, λ, be an eigenpair of (4.23) where we assume that $\lim_{\lambda\to 0} c/\lambda$ is finite and non-zero. Moreover, suppose that (6.4) holds. Then, Φ, λ is an eigenpair of (6.5). Alternatively, if Φ, λ is an eigenpair of (6.5) with $\lambda \neq 3$, then if $\lim_{\lambda\to 0} c/\lambda$ is finite and non-zero, this eigenpair is also an eigenpair of (4.23).*

Next, using (6.1) for c, and noting from the expression for χ_2 in (3.22b) that $\chi_2 = 0$ when $\lambda = 0$, we can eliminate the removable singularity at $\lambda = 0$ for χ, defined in (6.5), by rewriting

$$\chi = \frac{(\lambda-3)(2c_0+a)\int w^4}{b\int w^5 - \left(c_0\int w^4 + 1\right)(3-\lambda)}\,, \qquad \text{where} \qquad c_0 \equiv \frac{c}{\lambda} = \frac{2\hat{\chi}_2}{\int w^2}\,, \qquad \hat{\chi}_2 \equiv \frac{\chi_2}{\lambda} = -\frac{\chi_0\tau_u\kappa_2}{\tau_u\lambda+1}\,. \tag{6.9}$$

From (6.1), and by setting $q = 2$ in (3.22b), we obtain that the terms a and b in (6.9) are given explicitly by

$$a \equiv \frac{4\chi_0\kappa_2}{\int w^4}\,, \quad b \equiv \frac{3\chi_0}{\int w^3}\,, \quad \text{where} \quad \chi_0 \equiv \frac{1}{1+\kappa_2+\mathcal{D}_u}\,, \quad \kappa_2 = \frac{4U_0}{3\omega}\,, \quad \omega \equiv S(\gamma-\alpha) - \frac{4U_0}{3}\,. \tag{6.10}$$

In the usual way, it can be shown that the discrete spectra of the NLEP (6.5) are the roots of $\zeta(\lambda) = 0$ defined by

$$\zeta(\lambda) \equiv \mathcal{C}(\lambda) - \mathcal{F}(\lambda)\,, \tag{6.11a}$$

where

$$\mathcal{C}(\lambda) \equiv \frac{1}{\chi(\lambda)} = \frac{b\int w^5 - \left(c_0\int w^4 + 1\right)(3-\lambda)}{(\lambda-3)(2c_0+a)\int w^4}\,, \qquad \text{and} \qquad \mathcal{F}(\lambda) \equiv \frac{\int w^3\,(L_0-\lambda)^{-1}\,w^3}{\int w^4}\,. \tag{6.11b}$$

https://doi.org/10.1017/S0956792519000305 Published online by Cambridge University Press

By substituting (6.10) into (6.11b), we obtain after some rather lengthy, but straightforward, algebra that

$$\mathcal{C}(\lambda) = \frac{1}{2} + \frac{1}{4\kappa_2}\left(\frac{\tau_u\lambda + 1}{\tau_u\lambda + 1 - \frac{4\tau_u}{3}}\right)\left(1 + \mathcal{D}_u - \kappa_2 + \frac{9}{2(\lambda - 3)}\right). \tag{6.11c}$$

In addition, using $L_0 w = 2w^3$, we can more conveniently rewrite $\mathcal{F}(\lambda)$ in (6.11b) as

$$\mathcal{F}(\lambda) = \frac{1}{2\int w^4}\int w^3(L_0 - \lambda)^{-1}\left[(L_0 - \lambda) + \lambda\right] w = \frac{1}{2} + \frac{\lambda}{2\int w^4}\int w^3(L_0 - \lambda)^{-1} w\,. \tag{6.11d}$$

As a remark, we can use (6.11) to recover the competition stability threshold given in (5.2) when $q = 2$. To see this, we set $\lambda = 0$ in (6.11d) and (6.11c) to get $\mathcal{F}(0) = 1/2$ and

$$\mathcal{C}(0) = \frac{1}{2} + \frac{3}{4\kappa_2(3 - 4\tau_u)}\left[\mathcal{D}_u - \left(\kappa_2 + \frac{1}{2}\right)\right]. \tag{6.12}$$

Therefore, $\mathcal{C}(0) = 1/2$, so that $\zeta(0) = 0$ in (6.11a), when $\mathcal{D}_u = 1/2 + \kappa_2$. This zero-eigenvalue condition agrees with (5.2).

6.2 Parametrisation of the Hopf bifurcation threshold

In this subsection, we use (6.11) to determine an explicit parameterisation of any Hopf bifurcation for the NLEP (6.5). We set $\lambda = i\omega$, with $\omega > 0$, and obtain by setting $\zeta(i\omega) = 0$ in (6.11) that

$$\left(\frac{1 + i\omega\tau_u}{1 - \frac{4\tau_u}{3} + i\omega\tau_u}\right)\left(\frac{2}{9}\left(1 + \mathcal{D}_u - \kappa_2\right) + \frac{1}{i\omega - 3}\right) = \frac{8\kappa_2}{9}\left[\mathcal{F}(i\omega) - \frac{1}{2}\right]. \tag{6.13}$$

We then decompose $\mathcal{F}(i\omega)$ into real and imaginary parts to obtain from (6.11b) that

$$\mathcal{F}(i\omega) = \mathcal{F}_R(\omega) + i\mathcal{F}_I(\omega)\,, \quad \mathcal{F}_R(\omega) \equiv \frac{\int w^3 L_0\left[L_0^2 + \omega^2\right]^{-1} w^3}{\int w^4}\,, \quad \mathcal{F}_I(\omega) \equiv \omega\frac{\int w^3\left[L_0^2 + \omega^2\right]^{-1} w^3}{\int w^4}\,. \tag{6.14}$$

To determine a parameterisation of the Hopf bifurcation curve, we first multiply both sides of (6.13) by $i\omega\tau_u + 1 - 4\tau_u/3$, and then separate the resulting expression into real and imaginary parts. This yields that

$$\frac{2}{9}\left(1 + \mathcal{D}_u - \kappa_2\right) - \frac{3}{9 + \omega^2} + \frac{\tau_u\omega^2}{9 + \omega^2} = \frac{8\kappa_2}{9}\left(\mathcal{F}_R(\omega) - \frac{1}{2}\right)\left(1 - \frac{4\tau_u}{3}\right) - \frac{8\kappa_2\tau_u}{9}\omega\mathcal{F}_I(\omega)\,, \tag{6.15a}$$

$$\frac{2\tau_u\omega}{9}\left(1 + \mathcal{D}_u - \kappa_2\right) - \frac{3\tau_u\omega}{9 + \omega^2} - \frac{\omega}{9 + \omega^2} = \frac{8\kappa_2}{9}\left(\tau_u\omega\left[\mathcal{F}_R(\omega) - \frac{1}{2}\right] + \left(1 - \frac{4\tau_u}{3}\right)\mathcal{F}_I(\omega)\right). \tag{6.15b}$$

We then solve (6.15a) for $\mathcal{D}_u$ and substitute the resulting expression into (6.15b). This yields a quadratic equation for τ_u.

https://doi.org/10.1017/S0956792519000305 Published online by Cambridge University Press

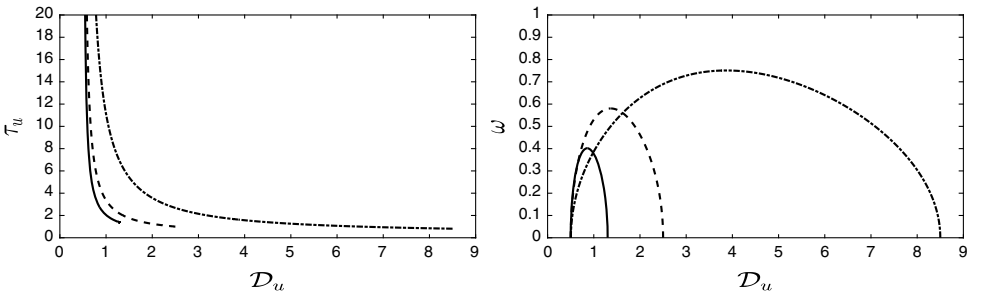

FIGURE 6. Left panel: the Hopf bifurcation threshold for 'cops-on-the-dots' in the τ_u vs. $\mathcal{D}_u$ plane, as computed from the parameterisation (6.16), for $U_0 = 2$ (solid curve), $U_0 = 3$ (dashed curve) and $U_0 = 4$ (dot-dashed curve) when $S = 6$, $\gamma = 2$ and $\alpha = 1$. Right panel: the corresponding Hopf bifurcation frequency ω vs. $\mathcal{D}_u$.

In this way, we obtain the following parameterisation, with parameter ω, for any Hopf bifurcation curve $\tau_u = \tau_u(\omega)$ and $\mathcal{D}_u = \mathcal{D}_u(\omega)$ for the NLEP (6.5):

$$\mathcal{D}_u = \kappa_2 - 1 + \frac{9}{2}\left(\frac{3}{9+\omega^2} + \frac{8\kappa_2}{9}\left[\mathcal{F}_R(\omega) - \frac{1}{2}\right] - \eta_0\tau_u\right), \tag{6.16a}$$

where τ_u is a root of the quadratic equation

$$\eta_0\tau_u^2 - \eta_1\tau_u + \eta_2 = 0\,. \tag{6.16b}$$

Here η_0, η_1 and η_2 are defined by

$$\eta_0 \equiv \frac{\omega^2}{9+\omega^2} + \frac{32\kappa_2}{27}\left[\mathcal{F}_R(\omega) - \frac{1}{2}\right] + \frac{8\kappa_2\omega}{9}\mathcal{F}_I(\omega)\,,$$
$$\eta_1 \equiv \frac{32\kappa_2}{27\omega}\mathcal{F}_I(\omega)\,, \qquad \eta_2 \equiv \frac{1}{9+\omega^2} + \frac{8\kappa_2}{9\omega}\mathcal{F}_I(\omega)\,. \tag{6.16c}$$

Since $\mathcal{F}_I(\omega) > 0$ for $\omega > 0$ (see part (v) of Proposition 4.3 in [22]), it follows that $\eta_1 > 0$ and $\eta_2 > 0$ for $\omega > 0$. However, the sign of η_0 is unclear, owing to the fact that $\mathcal{F}_R(\omega) < 1/2$ for $\omega > 0$ (see the left panel of Figure 4 of [22]).

To calculate the Hopf bifurcation curve, we fix $\kappa_2 > 0$ and let $\omega > 0$ be a parameter, and then numerically compute $\mathcal{F}_R(\omega)$ and $\mathcal{F}_I(\omega)$, as defined in (6.14), using a BVP solver. We then use (6.16b) to compute a $\tau_u > 0$, which determines $\mathcal{D}_u$ from (6.16a). In this way, in the left panel of Figure 6, we plot the Hopf bifurcation threshold τ_u vs. $\mathcal{D}_u$ for $U_0 = 2$, $U_0 = 3$ and $U_0 = 4$ for the fixed parameter set $S = 6$, $\gamma = 2$ and $\alpha = 1$. In addition, the Hopf frequency ω is plotted vs. $\mathcal{D}_u$ in the right panel of Figure 6. We emphasise that the Hopf curves in Figure 6 are universal in the sense that, together with the relation (3.23) and (3.24), they provide Hopf bifurcation thresholds for each of the asynchronous modes $j = 1, \ldots, K-1$ in the $\mathcal{D}_p$ vs. $\mathcal{D}$ parameter plane. In terms of these original parameters, the Hopf curves are plotted in Section 7, where we will also provide a detailed comparison of the linear stability results with full PDE numerical simulations of (1.4).

An interesting feature, as observed in Figure 6, is that the Hopf bifurcation frequency ω tends to zero at each of the two endpoints of the Hopf bifurcation curves, and that τ_u diverges at the lower endpoint in $\mathcal{D}_u$. To derive scaling laws for the Hopf thresholds at these two endpoints,

https://doi.org/10.1017/S0956792519000305 Published online by Cambridge University Press

we will take the limit $\omega \to 0$ in (6.16). To do so, we need the following lemma, as proved in Appendix B, which provides two-term expansions for $\mathcal{F}_R(\omega)$ and $\mathcal{F}_I(\omega)$ as $\omega \to 0$:

Lemma 6.3 *As $\omega \to 0$, and with $w(y) = \sqrt{2}\,\mathrm{sech}\, y$, the real and imaginary parts of $\mathcal{F}(i\omega)$, as defined in (6.14), have the asymptotics*

$$\mathcal{F}_R(\omega) \sim \frac{1}{2} - \frac{3}{64}\omega^2 + \mathcal{O}(\omega^4)\,; \qquad \mathcal{F}_I(\omega) \sim \frac{3\omega}{16} + d_I\omega^3\,, \qquad d_I \equiv -\frac{\int y^2(w')^2}{16\int w^4} \approx -0.0285\,. \tag{6.17}$$

We substitute (6.17) into (6.16c) to obtain expressions for η_0, η_1 and η_2 for $\omega \to 0$. In this way, for $\omega \to 0$, (6.16b) becomes a singularly perturbed quadratic equation for τ_u

$$\omega^2\tau_u^2\left[1+\kappa_2+\mathcal{O}(\omega^2)\right] - 2\kappa_2\tau_u\left(1+\frac{16}{3}d_I\omega^2+\mathcal{O}(\omega^4)\right)+1+\frac{3\kappa_2}{2}+\omega^2\left(8\kappa_2 d_I-\frac{1}{9}\right)+\mathcal{O}(\omega^4)=0\,. \tag{6.18}$$

For $\omega \to 0$, (6.18) has a small root with $\tau_u = \mathcal{O}(1)$ and a large root with $\tau_u = \mathcal{O}(\omega^{-2})$. By asymptotically calculating these two roots, and then using (6.16a) and (6.17) to determine $\mathcal{D}_u$, we readily obtain two scaling laws valid near each of the endpoints of the Hopf threshold curve shown in the left panel of Figure 6.

In this way, we find that the small root corresponds to the right-hand endpoint of the Hopf curve, and for $\omega \to 0$

$$\begin{aligned} \tau_u \sim \tau_0 + \omega^2\tau_1 + \cdots\,, \quad \mathcal{D}_u \sim \kappa_2 + \frac{1}{2} - \frac{\omega^2}{4}\left(\frac{19}{6}+\frac{9\kappa_2}{4}+\frac{1}{\kappa_2}\right)\,; \\ \mathcal{D}_u \sim \kappa_2 + \frac{1}{2} - \frac{(\tau-\tau_0)}{4\tau_1}\left(\frac{19}{6}+\frac{9\kappa_2}{4}+\frac{1}{\kappa_2}\right)\,, \end{aligned} \tag{6.19a}$$

where τ_0 and τ_1 are defined by

$$\tau_0 \equiv \frac{3}{4} + \frac{1}{2\kappa_2}\,, \qquad \tau_1 \equiv \frac{(1+\kappa_2)\,(1+3\kappa_2/2)^2}{8\kappa_2^3} - \frac{1}{18\kappa_2} - \frac{8d_I}{3\kappa_2}\,. \tag{6.19b}$$

In contrast, the large root of (6.18) corresponds to the left-hand endpoint of the Hopf curve. For $\omega \to 0$, we obtain

$$\tau_u \sim \left(\frac{2\kappa_2}{1+\kappa_2}\right)\omega^{-2} + \mathcal{O}(1)\,, \quad \mathcal{D}_u \sim \frac{1}{2} + \omega^2 b\,, \quad \text{where} \quad b \equiv \frac{11}{24} + \kappa_2\left(\frac{3}{16} - \frac{16}{3}d_I\right) + \frac{1}{4\kappa_2}\,. \tag{6.20}$$

This yields the key scaling law for the left endpoint of the Hopf curve that

$$\tau_u \sim \left(\frac{2\kappa_2}{1+\kappa_2}\right)\frac{b}{\mathcal{D}_u - 1/2}\,, \qquad \text{as} \qquad \mathcal{D}_u \to (1/2)^+\,. \tag{6.21}$$

In Figure 7, we compare the two asymptotic approximations (6.19) and (6.21) with results computed numerically from the parameterisation (6.16) for the same parameter values as in Figure 6. Rather remarkably, we observe that the asymptotic results provide a decent quantitative prediction of the *entire* Hopf bifurcation curve. This close agreement is due to the Hopf frequency ω being relatively small on the entire range of the Hopf curve (see the right panel of Figure 6).

https://doi.org/10.1017/S0956792519000305 Published online by Cambridge University Press

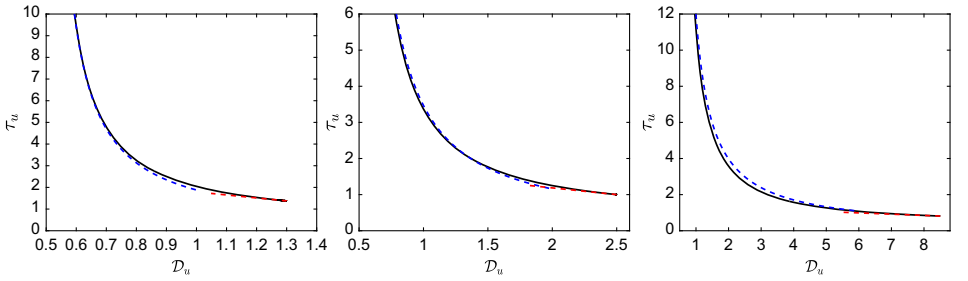

FIGURE 7. The Hopf bifurcation threshold for $U_0 = 2$ (left panel), $U_0 = 3$ (middle panel) and $U_0 = 4$ (right panel), when $S = 6$, $\gamma = 2$, and $\alpha = 1$, computed numerically from the parameterisation (6.16) (solid curves). The dashed curves are the asymptotics for small ω near the right endpoint (6.19) (red curves) and the left endpoint (6.21) (blue curves). The asymptotic approximations are seen to provide a good approximation to almost the entire Hopf bifurcation curve.

In Proposition 6.4 given below in Section 6.3, we prove that a multi-hotspot steady state is unstable whenever $\mathcal{D} > \mathcal{D}_c \equiv \kappa_2 + 1/2$ *for any* $\tau_u > 0$. This result is complementary to that in Section 5.1 where we proved a similar instability result for any $q > 1$, but with $\tau_u \to 0^+$. For the range $\mathcal{D} < \mathcal{D}_c$, we conjecture that the Hopf bifurcation curve in Figure 7 sets the linear stability boundary in the τ_u vs. $\mathcal{D}_u$ parameter space. This assertion is based on a continuation argument in τ_u. Recall from Proposition 5.2 that for $\tau_u \to 0^+$, the NLEP (3.22) has no unstable eigenvalues when $\mathcal{D} < \mathcal{D}_c$. By increasing τ_u for fixed $\mathcal{D}_u < \mathcal{D}_c$, our parameterisation (6.16) has shown that eigenvalues of (6.5) can occur on the imaginary axis $\lambda = i\omega$, with $\omega > 0$, only on the range $1/2 < \mathcal{D}_u < \mathcal{D}_c$. For $0 < \mathcal{D}_u < 1/2$, there are no purely imaginary eigenvalues for (6.5) for any $\tau_u > 0$, suggesting by continuity that $\mathrm{Re}(\lambda) \le 0$ for (6.5). This suggests that below the Hopf bifurcation curve, the multi-hotspot pattern is linearly stable, and that this hotspot steady state is linearly stable for all $\tau_u > 0$ when $\mathcal{D}_u < 1/2$. A computational tool to investigate this conjecture is formulated in Section 6.3.

6.3 An instability result and the winding number criterion

For the analysis below, for $\tau_u > 0$, it is convenient to express $\mathcal{C}(\lambda)$ in (6.11c) in terms of partial fractions as

$$\mathcal{C}(\lambda) = c_0 + \frac{c_1}{\lambda - 3} + \frac{c_2}{\lambda - \lambda_p}, \qquad \lambda_p \equiv \frac{4}{3} - \frac{1}{\tau_u}, \tag{6.22a}$$

where $\lambda_p > 0$ iff $0 < \tau_u < 3/4$. In (6.22a), the coefficients $c_0, c_1 > 0$ and c_2 are

$$\begin{aligned} c_0 &= \frac{1}{4}\left[1 + \frac{1}{\kappa_2}(1 + \mathcal{D}_u)\right], \quad c_1 = \frac{9}{8\kappa_2}\left(\frac{9\tau_u + 3}{5\tau_u + 3}\right), \\ c_2 &= \frac{1}{\kappa_2}\left(\frac{1}{5\tau_u + 3}\right)\left[(1 + \mathcal{D}_u - \kappa_2)\left(\frac{5\tau_u}{3} + 1\right) - \frac{9\tau_u}{2}\right]. \end{aligned} \tag{6.22b}$$

Our instability result is as follows:

Proposition 6.4 *For any $\tau_u > 0$, and for $q = 2$, a multi-hotspot steady-state solution is unstable to asynchronous perturbations of the hotspot amplitudes when $\mathcal{D} > \mathcal{D}_c \equiv \kappa_2 + 1/2$ and for any police diffusivity D_p on the range $\mathcal{O}(1) \ll D_p \ll \mathcal{O}(\epsilon^{-3})$.*

https://doi.org/10.1017/S0956792519000305 Published online by Cambridge University Press

Proof We need to prove that $\zeta(\lambda)$, defined in (6.11a), has a real positive root whenever $\tau_u > 0$ and $\mathcal{D} > \mathcal{D}_c$. To do so, we consider three ranges of τ_u. When $\tau_u < 3/4$, we have from (6.22a) that $\mathcal{C}(\lambda)$ is continuous on $0 < \lambda < 3$, with $\mathcal{C}(\lambda) \to -\infty$ as $\lambda \to 3^-$. In addition, from (6.12), we have $\mathcal{C}(0) > 1/2$ when $\mathcal{D} > \mathcal{D}_c$. From (6.11b), we have $\mathcal{F}(0) = 1/2$, $\mathcal{F}(\lambda)$ continuous on $0 < \lambda < 3$ and $\mathcal{F}(\lambda) \to +\infty$ as $\lambda \to 3^-$ (cf. [22]). Therefore, by the intermediate value theorem, there is a real root to $\zeta(\lambda) = 0$ on $0 < \lambda < 3$. When $\tau_u > 3/4$, (6.12) yields that $\mathcal{C}(0) < 1/2$ when $\mathcal{D}_u > \mathcal{D}_c$, while (6.22a) shows that $\mathcal{C}(\lambda)$ has a simple pole at $\lambda = \lambda_p \equiv 4/3 - 1/\tau_u$ in $0 < \lambda_p < 3$. Regardless of the sign of c_2 in (6.22b), it readily follows that $\zeta(\lambda) = 0$ has a real positive root in $0 < \lambda < 3$. Finally, suppose that $\tau_u = 3/4$. Then, from (6.22), we have that $\mathcal{C}(\lambda) \to c_2/\lambda$ as $\lambda \to 0$, with $c_2 = [\mathcal{D}_u - (\kappa_2 + 1/2)]/(3\kappa_2) > 0$ when $\mathcal{D}_u > \kappa_2 + 1/2$. Therefore, since $\mathcal{C}(\lambda) \to -\infty$ as $\lambda \to 3^-$, while $\mathcal{C}(\lambda) \to +\infty$ as $\lambda \to 0^+$ when $\mathcal{D}_u > \kappa_2 + 1/2$, it follows that $\zeta(\lambda) = 0$ has a root on $0 < \lambda < 3$. □

Next, we derive a winding number criterion that can be implemented numerically to count the number N of unstable eigenvalues of the NLEP (6.5). This hybrid analytical–numerical approach will be useful for considering the range $\mathcal{D} < \mathcal{D}_c$ and $\tau_u \neq 3/4$. For $\tau_u \neq 3/4$, $\mathcal{C}(\lambda)$ in (6.22) is analytic in $\mathrm{Re}(\lambda) \geq 0$ except for a simple pole at $\lambda = 3$, and an additional simple pole at $\lambda = \lambda_p > 0$ iff $\tau_u > 3/4$. From a winding number analysis, analogous to that developed in Section 5.1, the number N of roots of $\zeta(\lambda) = 0$ in $\mathrm{Re}(\lambda) > 0$, which is equivalent to the number of unstable eigenvalues of the NLEP (6.5), is

$$N = P + \frac{1}{\pi}\left[\arg \zeta\right]_{\Gamma_I^+}, \qquad P = \begin{cases} 1, & 0 < \tau_u < 3/4 \\ 2, & \tau_u > 3/4 \end{cases}. \tag{6.23a}$$

Here Γ_{I^+} is the positive imaginary axis traversed in the downwards direction. To numerically calculate $[\arg \zeta]_{\Gamma_I^+}$, we let $\lambda = i\omega$ with $\omega > 0$, and decompose $\zeta(i\omega) = \zeta_R(\omega) + i\zeta_I(\omega)$. Since $\zeta(i\omega) = \mathcal{C}(i\omega) - \mathcal{F}(i\omega)$, we use (6.14) for $\mathcal{F}(i\omega)$ together with (6.22) to calculate $\mathcal{C}(i\omega)$. This yields that

$$\begin{aligned} \zeta_R(\omega) &= c_0 - \frac{3c_1}{9+\omega^2} - \frac{\lambda_p c_2}{\lambda_p^2 + \omega^2} - \mathcal{F}_R(\omega), \\ \zeta_I(\omega) &= -\frac{\omega}{(9+\omega^2)(\lambda_p^2+\omega^2)}\left[(c_1+c_2)\,\omega^2 + c_1\lambda_p^2 + 9c_2\right] - \mathcal{F}_I(\omega). \end{aligned} \tag{6.23b}$$

Here $\mathcal{F}_R(\omega)$ and $\mathcal{F}_I\omega)$ can be calculated numerically from (6.14), while c_0, c_1 and c_2 are evaluated using (6.22b).

To illustrate the use of (6.23b), we consider the phase diagram in the τ_u vs. $\mathcal{D}_u$ shown in Figure 7 where $U_0 = 2$, $S = 6$, $\gamma = 2$, and $\alpha = 1$. There, we predicted that there are no unstable eigenvalues of the NLEP when $\mathcal{D}_u < 0.5$. For $0.5 < \mathcal{D}_u < \kappa_2 + 1/2 = 1.3$, we predicted that there are no unstable eigenvalues of the NLEP when τ_u is below the Hopf bifurcation threshold. For particular parameter values, in Figure 8, we show that a numerical implementation of the winding number criterion (6.3) confirms these predictions. Further numerical results using (6.3) for other parameter sets, and in particular for the middle and right panels of Figure 7, confirm the linear stability predictions of Section 6.2.

https://doi.org/10.1017/S0956792519000305 Published online by Cambridge University Press

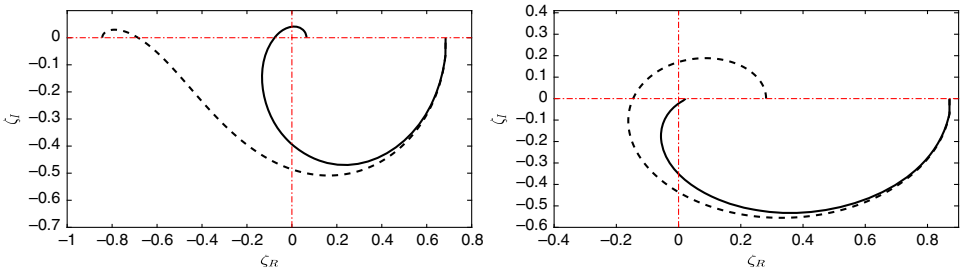

FIGURE 8. Plots of the path $\zeta(i\omega) = \zeta_R(\omega) + i\zeta_I(\omega)$ for $\mathcal{D}_u = 0.4$ (left panel) and $\mathcal{D}_u = 1.0$ (right panel) on $0 < \omega < \infty$, when $S = 6$, $\gamma = 2$ and $\alpha = 1$, corresponding to the left panel of Figure 7. Left panel: $\tau_u = 0.4$ (dashed curve), $\tau_u = 5.0$ (solid curve), for which $[\arg\zeta]_{\Gamma_I^+} = -\pi$ and $[\arg\zeta]_{\Gamma_I^+} = -2\pi$, respectively. For both values of τ_u, (6.23a) yields $N = 0$. Right panel: $\tau_u = 1.0$ (dashed curve), $\tau_u = 4.0$ (solid curve), for which $[\arg\zeta]_{\Gamma_I^+} = -2\pi$ and $[\arg\zeta]_{\Gamma_I^+} = 0$, respectively. Then, (6.23a) yields $N = 0$ for $\tau_u = 1.0$ and $N = 2$ for $\tau_u = 4.0$. These results are consistent with the linear stability phase diagram in the left panel of Figure 7.

7 Comparison of linear stability theory with PDE simulations: $q = 2$

We first map the phase diagrams for linear stability from the τ_u vs. $\mathcal{D}_u$ plane of Section 6 for $q = 2$ to that of the ϵD_p vs. $\mathcal{D}$ parameter plane. By setting $q = 2$ in (3.23) and (3.24), we obtain in terms of τ_u and $\mathcal{D}_u$ that

$$\mathcal{D} = \frac{\omega^3 S \mathcal{D}_u}{4K^4\alpha^2\pi^2\left[1-\cos\left(\frac{\pi j}{K}\right)\right]}, \qquad \epsilon D_p = \frac{S\omega^2}{K^3\alpha^2\pi^2\left[1-\cos\left(\frac{\pi j}{K}\right)\right]}\left(\frac{1}{\tau_u}\right), \quad \text{for} \quad j = 1,\ldots,K-1, \tag{7.1}$$

where $\omega = S(\gamma - \alpha) - 4U_0/3$. From (5.4), the competition instability threshold when $q = 2$ with $K \geq 2$ hotspots is

$$\mathcal{D}_c = \frac{\omega^3 S}{4K^4\alpha^2\pi^2\left[1+\cos\left(\pi/K\right)\right]}\left(\kappa_2 + \frac{1}{2}\right), \qquad \text{where} \qquad \kappa_2 = \frac{4U_0}{3\omega}. \tag{7.2}$$

The mapping (7.1), combined with the Hopf parameterisation in the τ_u vs. $\mathcal{D}_u$ plane as given by (6.16), is readily implemented numerically to determine a linear stability phase diagram in the ϵD_p vs. $\mathcal{D}$ parameter plane, representing the diffusivity of the police and criminals, respectively. For three different values of U_0, in Figure 9, we plot this linear stability phase diagram for a two-hotspot steady state for the parameter set $S = 6$, $\gamma = 2$ and $\alpha = 1$. A similar plot is shown in Figure 10 for a three-hotspot steady state.

For various points in the ϵD_p vs. $\mathcal{D}$ parameter plane, we now validate our linear stability results using the PDE software VLUGR [2] to compute full numerical simulations of the RD system (1.4) with 1000 meshpoints. For the initial condition for (1.4), we use a perturbation of the K-hotspot steady-state solution (see Corollary 2.2), given by

$$A(x,0) = \frac{1}{\epsilon\sqrt{v_0}}\sum_{j=1}^{K}\left(1+0.01a_j\right)w\left[\epsilon^{-1}(x-x_j)\right] + \alpha\left(1-\sum_{j=1}^{K}e^{-(x-x_j)^2/\epsilon^2}\right), \tag{7.3a}$$

https://doi.org/10.1017/S0956792519000305 Published online by Cambridge University Press

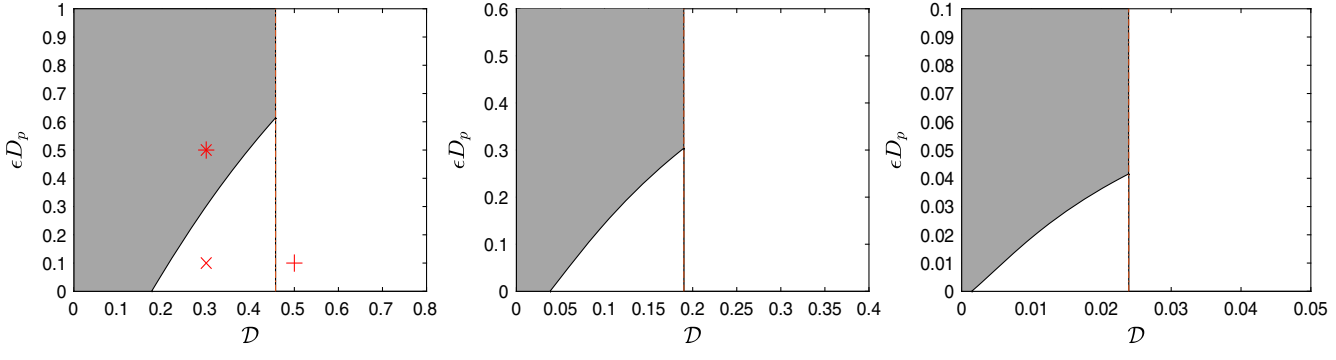

FIGURE 9. The linear stability phase diagram for a two-hotspot steady state in the ϵD_p vs. $\mathcal{D}$ parameter plane for cops-on-the-dots, as obtained from (7.1), when $S = 6$, $\gamma = 2$ and $\alpha = 1$. Left panel: $U_0 = 2$. Middle Panel: $U_0 = 3$. Right Panel: $U_0 = 4$. The thin vertical line in each panel is the competition stability threshold $\mathcal{D}_c$ of (7.2), which decreases rather substantially as U_0 increases. The shaded region is where the steady-state two-hotspot pattern is linearly stable. For $\mathcal{D} > \mathcal{D}_c$, the hotspot solution is unstable due to a competition instability, whereas in the unshaded region for $\mathcal{D} < \mathcal{D}_c$, the hotspot steady state is unstable to an asynchronous oscillatory instability of the hotspot amplitudes. PDE simulations of (1.4) at the marked points in the left panel are shown in Figure 11.

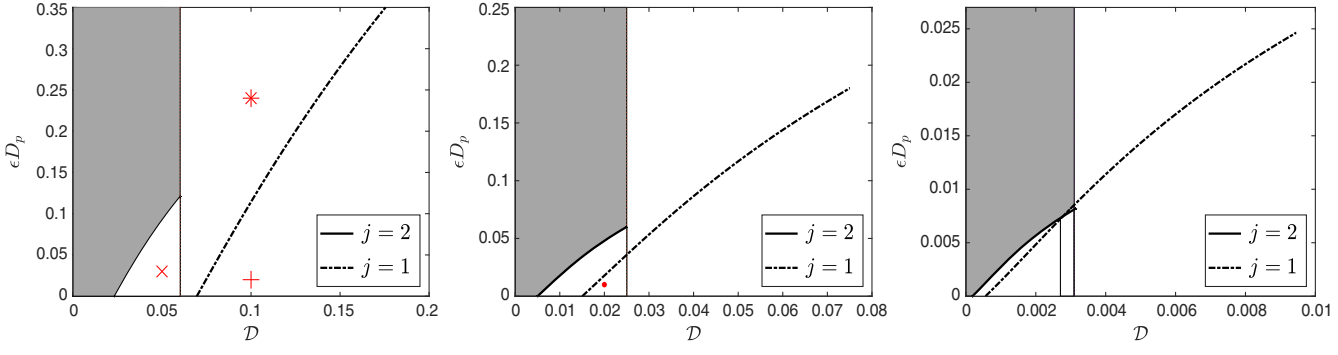

FIGURE 10. The linear stability phase diagram for a three-hotspot steady state in the ϵD_p vs. $\mathcal{D}$ parameter plane for cops-on-the-dots, as obtained from (7.1), when $S = 6$, $\gamma = 2$ and $\alpha = 1$. Left panel: $U_0 = 2$. Middle Panel: $U_0 = 3$. Right Panel: $U_0 = 4$. The three-hotspot steady state is linearly stable in the shaded region. The solid and dot-dashed curves are the Hopf bifurcation boundaries for the (sign-alternating) $j = 2$ mode and the $j = 1$ mode, respectively. This steady state undergoes an oscillatory instability below the solid or dot-dashed curves. In each panel, the thin vertical line at the right edge of the shaded region is the competition stability threshold $\mathcal{D}_c$ of (7.2). The additional thin vertical line in the right panel for $U_0 = 4$ is where the Hopf boundary switches from the $j = 2$ to the $j = 1$ mode. PDE simulations of (1.4) at the marked points in the left panel and at the marked point in the middle panel are shown in Figures 12 and 13, respectively.

$$\rho(x,0) = \sum_{j=1}^{K} \left(w[\epsilon^{-1}(x-x_j)]\right)^2, \qquad U(x,0) = \frac{U_0}{4\epsilon K} \sum_{j=1}^{K} \left(w[\epsilon^{-1}(x-x_j)]\right)^2, \tag{7.3b}$$

where the hotspot locations are at their steady-state values $x_j = S(2j-1)/(2K)$ for $j = 1, \ldots, K$. In (7.3b), the random coefficient a_j of the 1% perturbation of the hotspot amplitudes is taken to be uniformly distributed in $[-1, 1]$. For the PDE simulations reported below, we plot the amplitudes of the maxima of A vs. t for the baseline parameter set $S = 6$, $\gamma = 2$ and $\alpha = 1$.

For a two-hotspot solution, in Figure 11, we validate our linear stability predictions shown in the left panel of Figure 9 for $U_0 = 2$ and $\epsilon = 0.03$. The numerical results shown in Figure 11 suggest that the asynchronous hotspot oscillations, due to a Hopf bifurcation, and the competition instability, due to a positive real eigenvalue, are both subcritical instabilities.

For a three-hotspot solution, PDE simulations of (1.4) are shown in Figure 12 at each of the three marked points in the linear stability phase diagram given in the left panel of Figure 10. As discussed in the figure caption of Figure 12, these results again confirm the prediction of our linear stability analysis. For the parameter set corresponding to the middle panel of Figure 12, the hotspot steady state is unstable to both a competition instability, due to the sign-altering $j = 1$ mode, and an oscillatory instability for the $j = 2$ mode, which would lead to anti-phase oscillations between the first and third hotspots. However, since the linear growth rate for such anti-phase oscillations is rather small (see the right panel of Figure 6), the competition instability, which is due to a positive eigenvalue in the spectrum of the NLEP, is the dominant instability.

Finally, in Figure 13, we plot the numerically computed hotspot amplitudes, obtained from a PDE simulation of (1.4), at the marked point in the middle panel of Figure 10. For this parameter set, the three-hotspot steady state is unstable to both sign-altering ($j = 1$) and anti-phase ($j = 2$) temporal oscillations. The numerical results in Figure 13 show that the sign-altering mode is dominant and that small-amplitude oscillations persist over rather long time intervals. In contrast to the likely subcritical behaviour observed in the left panel of Figure 12, for this parameter set, the results in Figure 13 suggest a supercritical oscillatory instability.

8 Discussion

We focus here on summarising some of our main linear stability results for steady-state hotspot solutions of (1.4) for the special case $q = 2$ of 'cops-on-the-dots'; a PDE model originally derived in [10] from the continuum limit of an agent-based model of urban crime with police intervention. For $q = 2$, our hybrid asymptotic-numerical analysis of the NLEP linear stability problem has provided phase diagrams in the ϵD_p vs. $\mathcal{D}$ parameter space characterising the linear stability properties of multi-hotspot steady states for (1.4). For $\mathcal{D}$ exceeding the threshold $\mathcal{D}_c$ given by (7.2), called the competition stability threshold, we proved in Proposition 6.4 that multi-hotspot steady-state solutions are unstable for all police diffusivities D_p on the range $\mathcal{O}(1) \ll D_p \ll \mathcal{O}(\epsilon^{-3})$. On the intermediate range of $\mathcal{D}$ given by $\mathcal{D}^\star < \mathcal{D} < \mathcal{D}_c$, for some $\mathcal{D}^\star > 0$, our linear stability theory predicts that asynchronous hotspot amplitude oscillations will occur only if the police diffusivity is below some Hopf bifurcation threshold. In Section 4, and more specifically in Section 4.2.1, we have established through a detailed analysis of the additional NLEP given in (3.20) that a one-hotpot steady state is linearly stable, and that a multi-hotspot steady state is always linearly stable to synchronous perturbations of the hotspot amplitudes when

https://doi.org/10.1017/S0956792519000305 Published online by Cambridge University Press

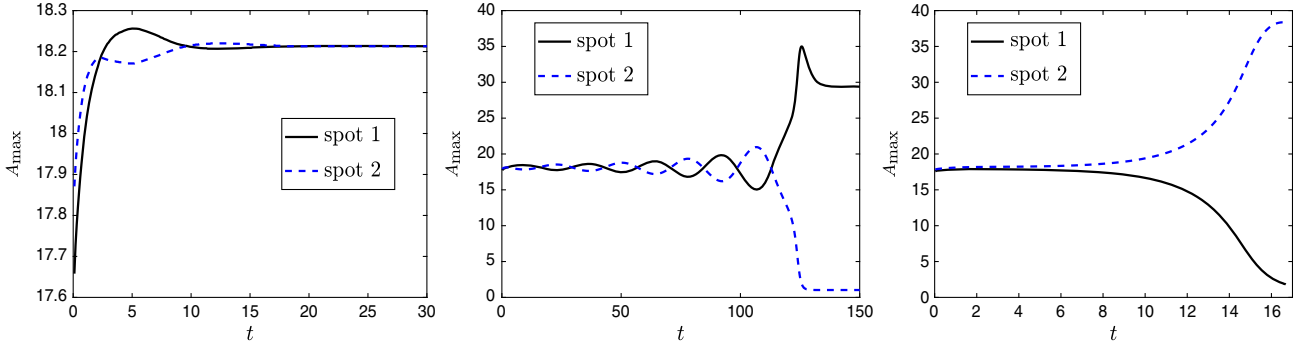

FIGURE 11. The hotspot amplitudes for A computed numerically from the full PDE system (1.4) for a two-spot pattern with $S = 6$, $\gamma = 2$, $\alpha = 1$, $U_0 = 2$, $\epsilon = 0.03$ and $q = 2$ (cops-on-the-dots), at each of the three marked points in the linear stability phase diagram shown in the left panel of Figure 9. Left panel: $\mathcal{D} = 0.3$ and $\epsilon D_p = 0.5$, so that $D_p \approx 16.67$ ($*$ point). The spot amplitudes are stable to asynchronous oscillations and to the competition instability. Middle panel: $\mathcal{D} = 0.3$ and $\epsilon D_p = 0.1$, so that $D_p \approx 3.33$ ($\times$ point). Spot amplitudes are unstable to asynchronous oscillations, leading to the oscillatory collapse of a hotspot. Right panel: $\mathcal{D} = 0.5$ and $\epsilon D_p = 0.1$, so that $D_p \approx 3.33$ ($+$ point). Spot amplitudes are unstable to a competition instability, leading to the monotonic collapse of a hotspot. These results are consistent with the linear stability predictions in the left panel of Figure 9.

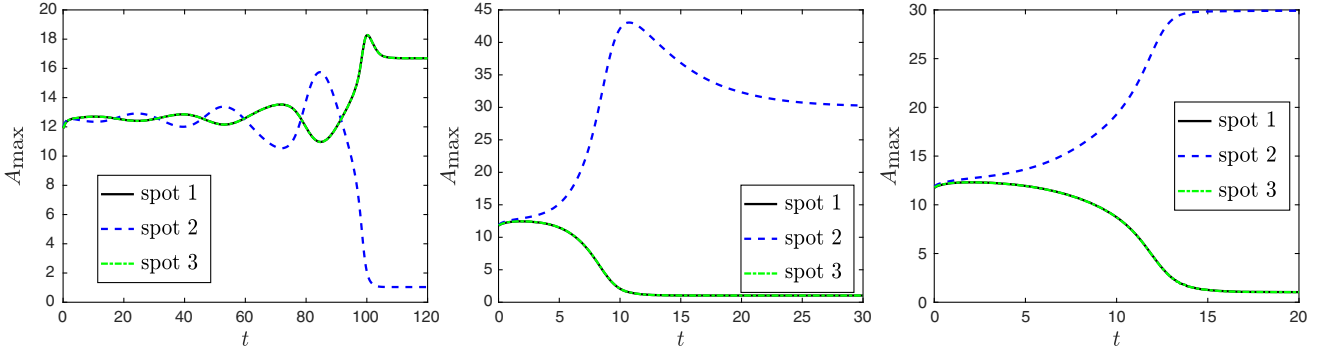

FIGURE 12. The hotspot amplitudes computed numerically from the full PDE system (1.4) for a three-spot pattern with $S = 6$, $\gamma = 2$, $\alpha = 1$, $U_0 = 2$, $\epsilon = 0.03$ and $q = 2$ (cops-on-the-dots), at each of the three marked points in the linear stability phase diagram shown in the left panel of Figure 10. Left panel: $\mathcal{D} = 0.05$ and $\epsilon D_p = 0.03$, so that $D_p = 1$ ($\times$ point). The spot amplitudes are unstable to asynchronous oscillations for the sign-altering $j = 1$ mode, which leads to the oscillatory collapse of the middle hotspot. The amplitudes of the first and third hotspots are essentially synchronised and trace out nearly identical curves. Middle panel: $\mathcal{D} = 0.1$ and $\epsilon D_p = 0.02$, so that $D_p \approx 0.667$ ($+$ point). Spot amplitudes are unstable to asynchronous oscillations to the $j = 2$ mode, and are unstable to a competition instability for the sign-altering $j = 1$ mode. The latter instability has a larger growth rate. An overshoot behaviour, followed by a collapse of the (essentially synchronous) first and third hotspots, is observed. Right panel: $\mathcal{D} = 0.1$ and $\epsilon D_p = 0.24$, so that $D_p = 8$ ($*$ point). Spot amplitudes are unstable to a competition instability for the sign-altering mode, but are now linearly stable to the $j = 2$ oscillatory mode. A monotonic collapse of the first and third hotspots is observed. These results are consistent with the linear stability predictions in the left panel of Figure 10.

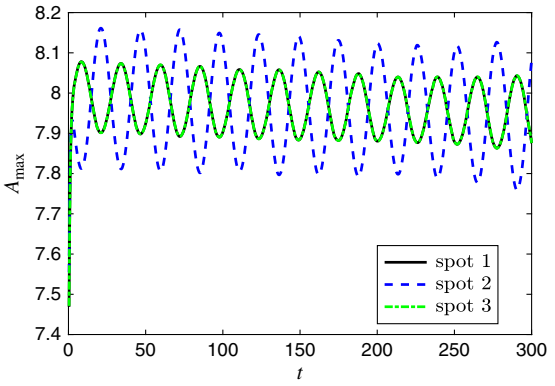

FIGURE 13. The hotspot amplitudes computed numerically from the full PDE system (1.4) for a three-spot pattern with $S=6$, $\gamma=2$, $\alpha=1$, $U_0=3$, $\epsilon=0.03$ and $q=2$ (cops-on-the-dots), at the marked point in the middle panel of the phase diagram in Figure 10 where $\mathcal{D}=0.02$ and $\epsilon D_p=0.01$, so that $D_p\approx 0.333$. The spot amplitudes are unstable to both asynchronous oscillations for the sign-altering $j=1$ mode and the anti-phase mode $j=2$. Long-lived small-amplitude temporal oscillations that synchronise the first and third hotspots are observed (indicated by nearly overlapping amplitudes for the first and third spots).

$\mathcal{O}(1)\ll D_p\ll\mathcal{O}(\epsilon^{-3})$. Finally, in Section 7, our linear stability predictions were validated from full PDE numerical simulations of (1.4).

For the case $q=2$ of 'cops-on-the-dots', we now compare the linear stability results obtained in [22] for the simple police interaction model, in which $-\rho U$ in (1.1b) is replaced by $-U$, with the results obtained herein for (1.4) for a predator-prey type police interaction. Although the overall qualitative shape of the various regions in the linear stability phase diagram of the ϵD_p vs. $\mathcal{D}$ parameter plane is similar for the two models, there are two key quantitative differences. Firstly, the competition instability threshold value of $\mathcal{D}$ for (1.4) can be written as (see (7.2) with $q=2$)

$$\mathcal{D}_c=\frac{S}{8K^4\pi^2\alpha^2\left[1+\cos\left(\pi/K\right)\right]}g(\omega)\,,\qquad \text{where}\qquad g(\omega)\equiv-\omega^3+2S(\gamma-\alpha)\omega^2\,,\quad \omega=S(\gamma-\alpha)-4U_0/3\,,\qquad (8.1)$$

on $0<U_0<U_{0,\max}\equiv 3S(\gamma-\alpha)/4$. For the simple police interaction model studied in [22], equation (8.1) still holds but with ω replaced by $\omega_s\equiv S(\gamma-\alpha)-U_0$ (see equation (4.10) of [22]). For a given parameter set and fixed policing level U_0, since $\omega<\omega_s$ it follows that $\mathcal{D}_c$ is smaller for (1.4) than for the RD model in [22]. Consequently, the range of $\mathcal{D}$ where a K-hotspot pattern with $K\geq 2$ is unstable for all police diffusivities D_p is larger for (1.4) than it is for the RD model in [22]. Secondly, with regard to asynchronous hotspot oscillations for a two-hotspot solution, we observe by comparing the left panel of Figure 9 with the left panel of Figure 22 of [22] that the range of ϵD_p where these oscillations occur is smaller for (1.4) than it is for the RD model studied in [22], although the corresponding interval of $\mathcal{D}$ is roughly similar. A similar conclusion holds for a three-hotspot steady-state solution (compare left panels of Figures 10 and 24 of [22]). This indicates that the parameter region where asynchronous hotspot oscillations occur is smaller for (1.4) than for the model in [22].

https://doi.org/10.1017/S0956792519000305 Published online by Cambridge University Press

8.1 Open problems and further directions

We now discuss a few open technical issues for our specific RD system (1.4). Firstly, in our NLEP linear stability analysis of (3.22) to characterise asynchronous hotspot amplitude oscillations, we focused primarily on the case $q = 2$ of 'cops-on-the-dots', where the identities (4.24) were central for recasting the NLEP (3.22) with three nonlocal terms into the NLEP (6.5) with only one nonlocal term proportional to $\int w^3 \Phi$. Since this special reduction is not available for $q \neq 2$, a full numerical approach on the NLEP (3.22) would be needed to determine any Hopf bifurcation threshold for asynchronous oscillations when $q \neq 2$. Secondly, our construction of the steady state for (1.4), and our derivation of the NLEP, required that $q > 1$. For $q = 1$, corresponding to a peripheral interdiction policing strategy (cf. [10]), the complicating feature of the analysis is that there is now a non-negligible police population density both within the core of a hotspot and in the outer region away from the hotspots. This makes the asymptotic construction of a hotspot steady state considerably more intricate and leads to an NLEP with a rather different structure. Thirdly, for $q = 2$, it would be worthwhile to undertake a weakly nonlinear analysis to characterise the local branching behaviour near a Hopf bifurcation point of the asynchronous hotspot amplitude oscillations. In contrast to the RD model of simple police interaction studied in [22], where only subcritical amplitude oscillations were found numerically, it appears that either subcritical or supercritical hotspot amplitude oscillations can occur for (1.4) (compare Figures 11 and 12 with Figure 13). The significance of analytically establishing the supercriticality of the Hopf bifurcation is that it would determine the parameter range where crime is only displaced temporally between neighbouring hotspots over very long time intervals, without achieving a reduction in the overall total crime.

An open problem with a wider scope would be to study hotspot patterns for the RD system (1.4) when the criminal diffusivity satisfies $D = \mathcal{O}(1)$. For the basic two-component crime model with no police intervention, on this range it was shown in [21] that new hotspots of criminal activity can nucleate from an otherwise quiescent, largely crime-free, background, near a saddle-node bifurcation point of hotspot equilibria. It would be interesting to analyse whether this 'peak-insertion' effect persists for (1.4) when the effect of police is included. Finally, it would be worthwhile to extend our 1-D analysis to a 2-D spatial domain to determine whether hotspot amplitudes in 2-D can undergo asynchronous temporal oscillations, leading to the temporal displacement of crime between neighbouring spatial regions.

8.2 Qualitative remarks: Role of police intervention

From our steady-state hotspot analysis, as summarised in Corollary 2.2, the criminal density in a hotspot region is independent of the policing level. However, the maxima of the attractiveness field do decrease if additional police are added (U_0 increases) or if their movement towards maxima of the attractiveness becomes more pronounced (q increases). In fact, there is a critical level $U_{0,\max}$ of policing for which no steady-state hotspot patterns can occur.

However, in the event that that the police deployment U_0 is fixed below the level required to eliminate the occurrence of any crime hotspot, the key issue is how should the movement of the police be directed so as to reduce the overall total crime in the region. It is readily shown that the total crime in the region at a given time is proportional to the number of observable crime hotspots that can exist on the region. As such, within the context of the model, the police effort should be directed to try to minimise the maximum number of *dynamically stable* steady-state

https://doi.org/10.1017/S0956792519000305 Published online by Cambridge University Press

hotspots that can occur for the given region, and more specifically to shrink the parameter regime where these hotspots are stable, and hence observable, in time.

The analysis in Section 5 showed that there is a critical value of the diffusivity of criminals, referred to as the competition stability threshold, such that a particular steady-state hotspot pattern is unstable if the criminal diffusivity exceeds this value. This critical value depends on the number of hotspots, the overall policing level and the police focus towards maxima of the attractiveness field. Given that, in our model, the movement of criminals is not directly influenced by the police (i.e. $\mathcal{D}$ is a constant), the goal to decrease the overall amount of crime (i.e. the maximum number of stable hotspots) was to reduce this critical threshold of the criminal diffusivity by varying the policing level and police focus. Paradoxically, we showed that an overzealous policing effort focused on the hotspot regions (q increasing) is not beneficial to reducing the maximum number of observable crime hotspots when the overall level of police deployment is too low.

When the criminal diffusivity is below, but sufficiently close to, the competition stability threshold, in the context of our model the only strategy to decrease the number of observable crime hotspots is for the police to focus their movement towards observable hotspots in a sufficiently sluggish way (smaller D_p). With this strategy, we have shown that temporal oscillations in the amplitudes of the hotspots can be initiated, which has the effect of initiating a periodic-in-time displacement of crime between adjacent spatial regions. A problem left open in our study is to determine whether this temporal periodic sloshing in the intensity of adjacent crime hotspots eventually leads to the destruction of certain hotspots, and consequentially an overall reduction in total crime, or in fact persists for all time. However, the existence of oscillatory dynamics in the intensity of the hotspots is qualitatively consistent with field observations reported in [3] for a 'cops-on-the-dots' policing strategy. Finally, we remark that if the criminal diffusivity is sufficiently below the competition threshold, our phase diagrams have shown that no police intervention will be useful for reducing the overall total crime.

Acknowledgements

T. Kolokolnikov, M. J. Ward and J. Wei gratefully acknowledge the support of the NSERC Discovery Grant Program. A. Buttenschoen was partially supported by an NSERC PDF Fellowship. M. J. Ward would like to thank Dr. Wang Hung (Simon) Tse for some preliminary discussions on the analysis of this model.

Conflicts of interest

The authors declare that there are no conflict of interests with the undertaking of this research and with the publication of this article.

References

[1] BERESTYCKI, H., WEI, J. & WINTER, M. (2014) Existence of symmetric and asymmetric spikes for a crime hotspot model. *SIAM J. Math. Anal.*, **46**(1), 691–719.

[2] BLOM, J. G., TROMPERT, R. A. & VERWER, J. G. (1996) Algorithm 758: VLUGR 2: A vectorizable adaptive grid solver for PDEs in 2D. *ACM Trans. Math. Softw.*, **22**(3), 302–328.

[3] BRAGA, A. A. (2001) The effects of hot spots policing on crime. *Ann. Am. Acad. Polit. S. S.*, **578**, 104–125.

https://doi.org/10.1017/S0956792519000305 Published online by Cambridge University Press

[4] BRANTINGHAM, P. L. & BRANTINGHAM, P. J. (1987) *Crime Patterns*, McMillan.
[5] CAMACHO, A., LEE, H. R. L. & SMITH, L. (2016) Modeling policing strategies for departments with limited resources. *Europ. J. Appl. Math.*, **27**(3), 479–501.
[6] CANTRELL, R., COSNER, C. & MANASEVICH, R. (2012) Global bifurcation of solutions for crime modeling equations. *SIAM J. Math. Anal.* **44**(3), 1340–1358.
[7] DOELMAN, A., GARDNER, R. A. & KAPER, T. J. (2001) Large stable pulse solutions in reaction-diffusion equations. *Indiana U. Math. J.*, **50**(1), 443–507.
[8] GU, Y., WANG, Q. & YI, G. (2017) Stationary patterns and their selection mechanism of urban crime models with heterogeneous near-repeat victimization effect. *Europ. J. Appl. Math.*, **28**(1), 141–178.
[9] JOHNSON, S. & BOWER, K. (2005) Domestic burglary repeats and space-time clusters: The dimensions of risk. *Europ. J. of Criminology*, **2**, 67–92.
[10] JONES, P. A., BRANTINGHAM, P. J. & CHAYES, L. (2010) Statistical models of criminal behavior: The effect of law enforcement actions. *Math. Models. Meth. Appl. Sci.*, **20**, (Suppl.), 1397–1423.
[11] KOLOKOLNIKOV, T., WARD, M. J. & WEI, J. (2014) The stability of steady-state hot-spot patterns for a reaction-diffusion model of urban crime. *DCDS-B*, **19**(5), 1373–1410.
[12] KOLOKOLNIKOV, T., WARD, M. J. & WEI, J. (2005) The existence and stability of spike equilibria in the one-dimensional Gray-Scott model: the low feed rate regime. *Studies Appl. Math.*, **115**(1), 21–71.
[13] LLOYD, D. J. B. & O'FARRELL, H. (2013) On localised hotspots of an urban crime model. *Physica D*, **253**, 23–39.
[14] VAN DER PLOEG, H. & DOELMAN, A. (2005) Stability of spatially periodic pulse patterns in a class of singularly perturbed reaction-diffusion equations. *Indiana Univ. Math. J.*, **54**(5), 1219–1301
[15] PITCHER, A. B. (2010) Adding police to a mathematical model of burglary. *Europ. J. Appl. Math.*, **21**(4–5), 401–419.
[16] RICKETSON, L. (2011) A continuum model of residential burglary incorporating law enforcement, unpublished. Retrieved from http://cims.nyu.edu/~lfr224/writeup.pdf.
[17] RODRIGUEZ, N. & BERTOZZI, A. (2010) Local existence and uniqueness of solutions to a PDE model for criminal behavior, *M3AS (Special Issue on Mathematics and Complexity in Human and Life Sciences)*, **20**(1), 1425–1457.
[18] SHORT, M. B., D'ORSOGNA, M. R., PASOUR, V. B., TITA, G. E., BRANTINGHAM, P. J., BERTOZZI, A. L. & CHAYES, L. B. (2008) A statistical model of criminal behavior. *Math. Models. Meth. Appl. Sci.*, **18**(Suppl.), 1249–1267.
[19] SHORT, M. B., BERTOZZI, A. L. & BRANTINGHAM, P. J. (2010) Nonlinear patterns in urban crime – hotspots, bifurcations, and suppression. *SIAM J. Appl. Dyn. Sys.*, **9**(2), 462–483.
[20] SHORT, M. B., BRANTINGHAM, P. J., BERTOZZI, A. L. & TITA, G. E. (2010). Dissipation and displacement of hotpsots in reaction-diffusion models of crime. *Proc. Nat. Acad. Sci.*, **107**(9), 3961–3965.
[21] TSE, W.-H. & WARD, M. J. (2016) Hotspot formation and dynamics for a continuum model of urban crime. *Europ. J. Appl. Math.*, **27**(3), 583–624.
[22] TSE, W.-H. & WARD, M. J. (2018) Asynchronous instabilities of crime hotspots for a 1-D reaction-diffusion model of urban crime with focused police patrol. *SIAM J. Appl. Dyn. Sys.*, **17**(3), 2018–2075.
[23] TSE, W. H. (2016) Localized pattern formation in continuum models of urban crime, *Ph. D thesis*, Univ. of British Columbia.
[24] WARD, M. J. & WEI, J. (2003) Hopf bifurcations and oscillatory instabilities of spike solutions for the one-dimensional Gierer-Meinhardt model. *J. Nonlinear Sci.*, **13**(2), 209–264.
[25] WARD, M. J. & WEI, J. (2003) Hopf bifurcation of spike solutions for the shadow Gierer-Meinhardt model. *Europ. J. Appl. Math.* **14**(6), 677–711.
[26] WEI, J. & WINTER, M. (2003) A nonlocal eigenvalue problem and the stability of spikes for reaction-diffusion systems with fractional reaction rates. *Int. J. Bifur. Chaos* **13**(6), 1529–1543.
[27] WEI, J. & WINTER, M. (2001) Spikes for the two-dimensional Gierer-Meinhardt system: the weak coupling case. *J. Nonlinear Sci.*, **11**(6), 415–458.
[28] WEI, J. (1999) On single interior spike solutions for the Gierer-Meinhardt system: uniqueness and stability estimates. *Europ. J. Appl. Math.*, **10**(4), 353–378.

[29] WEI, J. (2008) Existence and stability of spikes for the Gierer-Meinhardt system. In: M. Chipot (editor), *Handbook of Differential Equations, Stationary Partial Differential Equations*, Vol. 5 , Elsevier, pp. 489–581.
[30] WILSON, J. Q. & KELLING, G. L. (1998) Broken windows and police and neighborhood safety. *Atlantic Mon.*, **249**, 29–38.
[31] ZIPKIN, J. R., SHORT, M. B. & BERTOZZI, A. L. (2014) Cops on the dots in a mathematical model of urban crime and police response. *DCDS-B*, **19**(5), 1479–1506.

Appendix A Derivation of the jump conditions: The NLEP

In this appendix, we derive the BVPs (3.7) and (3.9), with jump conditions, that are needed to obtain the NLEP (3.22).

To derive the BVP (3.7) with a jump condition for ψ_x across the hotspot region, we integrate (3.2b) over an intermediate domain $-\delta < x < \delta$ with $\epsilon \ll \delta \ll 1$. We use the facts that $A_e \sim \epsilon^{-1} w/\sqrt{v_0}$, $\phi \sim \Phi(y)$, $A_e(\pm\delta) \sim \alpha$ and $u_e = \epsilon^{q-1}\tilde{u}_e$ as given in (2.14), to obtain, upon letting $\delta/\epsilon \to +\infty$, that

$$\epsilon \mathcal{D}\alpha^2\,[\psi_x]_0 + 2\mathcal{D}\alpha\,[v_{ex}\phi]_0 = 3\epsilon \int_{-\infty}^{\infty} w^2\Phi\,dy + \frac{\epsilon\psi(0)}{v_0^{3/2}}\int_{-\infty}^{\infty} w^3\,dy + \frac{\epsilon(q+2)\tilde{u}_e}{v_0^{(q-1)/2}}\int_{-\infty}^{\infty} w^{q+1}\Phi\,dy + \frac{\epsilon\tilde{u}_e\psi(0)}{v_0^{1+q/2}}\int_{-\infty}^{\infty} w^{q+2} + \frac{\epsilon\eta(0)}{v_0^{q/2}}\int_{-\infty}^{\infty} w^{q+2}\,dy + \mathcal{O}(\epsilon^2\lambda)\,,$$

where we have introduced the notation $[a]_0 \equiv a(0^+) - a(0^-)$ to indicate that the evaluation is to be done with the outer solution. In addition, we have used the shorthand notation that $\int(\dots) \equiv \int_{-\infty}^{\infty}(\dots)\,dy$. Since $\phi = \mathcal{O}(\epsilon^3)$ in the outer region from (3.6), we can neglect the second term on the left-hand side of the expression above. For eigenvalues for which $\lambda \ll \mathcal{O}(\epsilon^{-1})$, the expression above simplifies to

$$\mathcal{D}\alpha^2[\psi_x]_0 = 3\int w^2\Phi + \frac{\psi(0)}{v_0^{3/2}}\int w^3 + \frac{(q+2)\tilde{u}_e}{v_0^{(q-1)/2}}\int w^{q+1}\Phi + \frac{\tilde{u}_e\psi(0)}{v_0^{1+q/2}}\int w^{q+2} + \frac{\eta(0)}{v_0^{q/2}}\int w^q\,. \tag{A.1}$$

Then, in (3.2b), we use $\phi = \mathcal{O}(\epsilon^3)$ in the outer region from (3.6), together with the fact $\epsilon^q\eta A_e^q \ll \mathcal{O}(\epsilon)$ since $q > 1$. In this way, (3.2b) and (A.1) yield the leading-order BVP problem for ψ given in (3.7) with a jump condition for ψ_x across $x = 0$:

To formulate a similar BVP for $\eta(x)$, we integrate (3.2c) over $-\delta < x < \delta$, with $\epsilon \ll \delta \ll 1$, and let $\delta/\epsilon \to \infty$ to obtain

$$\mathcal{D}\alpha^q\,[\eta_x]_0 + \mathcal{D}q\alpha^{q-1}\mathcal{O}(\epsilon^2) = \epsilon^{3-q}\tau\lambda\left[\frac{q\tilde{u}_\epsilon}{v_0^{(q-1)/2}}\int w^{q-1}\Phi + \frac{\eta(0)}{v_0^{q/2}}\int w^q\right]. \tag{A.2}$$

Moreover, in the outer region, we obtain from (3.2c) that

$$\mathcal{D}\alpha^q\eta_{xx} + \mathcal{O}(\epsilon^2) = \epsilon^2\tau\lambda\left[\alpha^q\eta + \mathcal{O}(\epsilon^2)\right]. \tag{A.3}$$

https://doi.org/10.1017/S0956792519000305 Published online by Cambridge University Press

For $\lambda = \mathcal{O}(1)$, we can neglect the $\mathcal{O}(\epsilon^2)$ term on the left-hand side of the jump condition (A.2) when $\mathcal{O}(\epsilon^2) \ll \mathcal{O}(\epsilon^{3-q}\tau)$, which implies that $\tau \gg \mathcal{O}(\epsilon^{q-1})$. On this range of τ, we obtain the jump condition

$$\mathcal{D}\alpha^q \left[\eta_x\right]_0 \sim \epsilon^{3-q}\tau\lambda \left[\frac{q\tilde{u}_e}{v_0^{(q-1)/2}} \int w^{q-1}\Phi + \frac{\eta(0)}{v_0^{q/2}} \int w^q \right] . \tag{A.4}$$

Likewise, when $\lambda = \mathcal{O}(1)$, we have from (A.3) that $\eta_{xx} \approx 0$ to leading order in the outer region when $\tau \ll \mathcal{O}(\epsilon^{-2})$. Therefore, upon combining these two bounds, in our analysis for $q > 1$ we will consider the parameter range

$$\mathcal{O}(\epsilon^{q-1}) \ll \tau \ll \mathcal{O}(\epsilon^{-2}) . \tag{A.5}$$

Upon using $D_p = \epsilon^{-2}\mathcal{D}/\tau$, (A.5) implies the following range of the police diffusivity:

$$\mathcal{O}(1) \ll D_p \ll \mathcal{O}(\epsilon^{-1-q}) . \tag{A.6}$$

Finally, by introducing the new variable $\hat{\tau}$ by $\hat{\tau} \equiv \epsilon^{3-q}\tau$, we obtain from (A.4) that

$$\mathcal{D}\alpha^q \left[\eta_x\right]_0 \sim \hat{\tau}\lambda \left[\frac{q\tilde{u}_e}{v_0^{(q-1)/2}} \int w^{q-1}\Phi + \frac{\eta(0)}{v_0^{q/2}} \int w^q \right] . \tag{A.7}$$

From (A.5), we obtain that both the jump conditions (A.7) hold and that $\eta_{xx} \approx 0$ in the outer region when $\hat{\tau}$ satisfies

$$\mathcal{O}(\epsilon^2) \ll \hat{\tau} \ll \mathcal{O}(\epsilon^{1-q}) , \tag{A.8}$$

where $q > 1$. For this range of $\hat{\tau}$, which implies the range (A.6) for the police diffusivity, we obtain the BVP (3.9) for $\eta(x)$ with the specified jump condition for η_x across $x = 0$. We remark that when $\hat{\tau} = \epsilon^{3-q}\tau$, the police diffusivity D_p is $D_p = \mathcal{O}(\epsilon^{1-q})$, which is a specific scaling law on the range given in (A.6).

Appendix B Proof of lemma 6.3

We first determine $\mathcal{F}_R(\omega)$ in (6.14) for $\omega \to 0$. We use $(L_0^2 + \omega^2)^{-1} = L_0^{-2} - \omega^2 L_0^{-4} + \mathcal{O}(\omega^4)$ for $\omega \to 0$, to obtain that

$$\mathcal{F}_R(\omega) = \frac{\int w^3 L_0^{-1} w^3}{\int w^4} - \omega^2 \frac{\int w^3 L_0^{-3} w^3}{\int w^4} + \mathcal{O}(\omega^4) . \tag{B.1}$$

Since $L_0^{-1} w = \frac{1}{2}\left(w + yw'\right)$ and $L_0^{-1} w^3 = w/2$ (see equation (3.7) of [24]), we get using integration by parts that

$$\begin{aligned} \mathcal{F}_R(\omega) &= \frac{1}{2} - \frac{\omega^2}{2\int w^4} \int w^3 L_0^{-2} w + \mathcal{O}(\omega^4) = \frac{1}{2} - \frac{\omega^2}{2\int w^4} \int \left(L_0^{-1} w^3\right)\left(L_0^{-1} w\right) + \mathcal{O}(\omega^4) , \\ &= \frac{1}{2} - \frac{\omega^2}{8\int w^4} \int w\left(w + yw'\right) + \mathcal{O}(\omega^4) = \frac{1}{2} - \frac{\omega^2}{8\int w^4}\left[\int w^2 + \frac{1}{2}\int y\left(w^2\right)'\right] . \end{aligned} \tag{B.2}$$

https://doi.org/10.1017/S0956792519000305 Published online by Cambridge University Press

Upon integrating the last expression in (B.2) by parts, and then using $\int w^2/\int w^4 = 3/4$ from (2.5), we conclude that

$$\mathcal{F}_R(\omega) = \frac{1}{2} - \frac{\omega^2 \int w^2}{16 \int w^4} + \mathcal{O}(\omega^4) = \frac{1}{2} - \frac{3\omega^2}{64} + \mathcal{O}(\omega^4)\,, \qquad \text{as} \quad \omega \to 0\,. \tag{B.3}$$

This yields the result for $\mathcal{F}_R(\omega)$ given in (6.17) of Lemma 6.3.

Next, we derive the asymptotics of $\mathcal{F}_I(\omega)$ as $\omega \to 0$. By letting $\omega \to 0$ in (6.14) for $\mathcal{F}_I$, we obtain that

$$\mathcal{F}_I(\omega) = \omega \frac{\int w^3 L_0^{-2} w^3}{\int w^4} - \omega^3 \frac{\int w^3 L_0^{-4} w^3}{\int w^4} + \mathcal{O}(\omega^5)\,. \tag{B.4}$$

Upon integrating by parts, and then using $L_0^{-1} w^3 = w/2$, we obtain that

$$\begin{aligned} \mathcal{F}_I(\omega) &= \omega \frac{\int \left(L_0^{-1} w^3\right)^2}{\int w^4} - \omega^3 \frac{\int \left(L_0^{-1} w^3\right)\left(L_0^{-3} w^3\right)}{\int w^4} + \mathcal{O}(\omega^5) \\ &= \frac{\omega}{4} \frac{\int w^2}{\int w^4} - \frac{\omega^3}{2 \int w^4} \int w L_0^{-2} \left(L_0^{-1} w^3\right) + \mathcal{O}(\omega^5)\,. \end{aligned} \tag{B.5}$$

Next, we use $L_0^{-1} w^3 = w/2$, $\int w^2/\int w^4 = 3/4$ and $\int w L_0^{-2} w = \int \left(L_0^{-1} w\right)^2$ from integration by parts. Then, (B.5) becomes

$$\mathcal{F}_I(\omega) = \frac{3\omega}{16} - \frac{\omega^3}{4 \int w^4} \int \left(L_0^{-1} w\right)^2 + \mathcal{O}(\omega^5)\,. \tag{B.6}$$

Finally, we use $L_0^{-1} w = (w + y w')/2$, so that upon integration by parts (B.6) becomes

$$\begin{aligned} \mathcal{F}_I(\omega) &= \frac{3\omega}{16} - \frac{\omega^3}{16 \int w^4} \left[\int w^2 + \int y (w^2)' + \int y^2 (w')^2 \right] + \mathcal{O}(\omega^5) \\ &= \frac{3\omega}{16} - \frac{\omega^3}{16 \int w^4} \int y^2 (w')^2 + \mathcal{O}(\omega^5)\,. \end{aligned} \tag{B.7}$$

This completes the derivation of the two-term expansion of $\mathcal{F}_I(\omega)$ as $\omega \to 0$ given in (6.17) of Lemma 6.3. Using $\int w^4 = 16/3$ and $w = \sqrt{2}\,\mathrm{sech}(y)$, a numerical quadrature yields that $\mathcal{F}_I(\omega) = 3\omega/16 + d_I \omega^3 + \mathcal{O}(\omega^5)$, with $d_I \approx -0.0285$.

Appendix C Proof of lemma 4.1

In this appendix, we prove Lemma 4.1, i.e. we establish the following inequality

$$I_0[\Phi] = \int \left[(\Phi')^2 + \Phi^2 - 3 w^2 \Phi^2\right] + 3 \frac{\int w^3 \Phi \int w^2 \Phi}{\int w^3} > 0\,, \quad \forall \Phi \not\equiv 0\,. \tag{C.1}$$

To this end, we consider the following quadratic form

$$Q_a[\Phi] \equiv \int \left[(\Phi')^2 + \Phi^2 - 3 w^2 \Phi^2\right] + 2a \frac{\int w^3 \Phi \int w^2 \Phi}{\int w^3} + 2b \frac{(\int w^3 \Phi)^2}{\int w^4}\,, \tag{C.2}$$

https://doi.org/10.1017/S0956792519000305 Published online by Cambridge University Press

where

$$b = \frac{5}{4} - a\,. \tag{C.3}$$

By setting $p = 3$ in Lemma 5.3 (2) of [28], we infer that

$$\int [(\Phi')^2 + \Phi^2 - 3w^2\Phi^2] + 2\frac{\left(\int w^3\Phi\right)^2}{\int w^4} > 0\,, \tag{C.4}$$

and hence $Q_0[\Phi] > 0$ (since $2b = 5/2 > 2$ when $a = 0$). Next, we observe that $Q_a[\Phi] = -\int \Phi\mathcal{L}\Phi$, where $\mathcal{L}$ is the self-adjoint linear operator

$$\mathcal{L}\Phi \equiv L_0\Phi - \left(a\frac{\int w^2\Phi}{\int w^3} + 2b\frac{\int w^3\Phi}{\int w^4}\right)w^3 - a\frac{\int w^3\Phi}{\int w^3}w^2\,. \tag{C.5}$$

We will continue in the parameter a until we reach a point for which $\mathcal{L}$ has principal eigenvalue zero, i.e. there exists an eigenfunction satisfying $\mathcal{L}\Phi = 0$ for some $\Phi \not\equiv 0$. At this point, $Q_a[\Phi]$ ceases to be positive definite.

To study this zero-eigenvalue problem, we set $c_1 = \int w^3\Phi$ and $c_2 = \int w^2\Phi$. We will use the identities $L_0^{-1}w^3 = \frac{1}{2}w$, $L_0^{-1}w^2 = \frac{1}{3}w^2$, $\int w^3L_0^{-1}w^2 = \int w^2L_0^{-1}w^3 = \frac{1}{2}\int w^3$ and $\int w^2L_0^{-1}w^2 = \frac{1}{3}\int w^4$. Upon multiplying $\mathcal{L}\Phi = 0$ in (C.5) by w and integrating by parts, we get

$$c_1 = \left(a\frac{c_2}{\int w^3} + 2b\frac{c_1}{\int w^4}\right)\frac{\int w^4}{2} + \frac{a}{2}\frac{c_1}{\int w^3}\int w^3\,, \tag{C.6}$$

which yields

$$\left(b + \frac{a}{2} - 1\right)c_1 + \frac{a}{2}\frac{\int w^4}{\int w^3}c_2 = 0\,. \tag{C.7}$$

Similarly, we multiply $\mathcal{L}\Phi = 0$ by w^2 and integrate by parts to get

$$c_2 = \left(a\frac{c_2}{\int w^3} + 2b\frac{c_1}{\int w^4}\right)\frac{\int w^5}{3} + \frac{a}{3}\frac{c_1}{\int w^3}\int w^4\,. \tag{C.8}$$

Upon using $\int w^5 = (3/2)\int w^3$, (C.8) becomes

$$\left(\frac{a}{3}\frac{\int w^4}{\int w^3} + b\frac{\int w^3}{\int w^4}\right)c_1 + \left(\frac{a}{2} - 1\right)c_2 = 0\,. \tag{C.9}$$

The homogeneous linear system (C.7) and (C.9) for c_1 and c_2 has a nontrivial solution if and only if $H(a) = 0$, where

$$H(a) \equiv \left(b + \frac{a}{2} - 1\right)\left(\frac{a}{2} - 1\right) - \frac{a^2}{6}\left(\frac{\int w^4}{\int w^3}\right)^2 - \frac{ab}{2}\,. \tag{C.10}$$

Recalling the choice of b in (C.3), and using $\int w^4 = 16/3$ and $\int w^3 = \sqrt{2}\pi$, we readily calculate from (C.10) that

$$H(a) = -\frac{1}{4} + \left(\frac{1}{4} - \frac{64}{27\pi^2}\right)a^2\,. \tag{C.11}$$

We calculate that $H(0) < 0$ and $H(2) < 0$, so that $H(a) < 0$ for $a \in [0, 2]$.

https://doi.org/10.1017/S0956792519000305 Published online by Cambridge University Press

In this way, we conclude that $Q_{\frac{3}{2}}[\Phi] > 0 \ \forall \Phi \not\equiv 0$, which means that

$$Q_{\frac{3}{2}}[\Phi] := \int \left[\left(\Phi'\right)^2 + \Phi^2 - 3w^2\Phi^2 \right] + 3\frac{\int w^3\Phi \int w^2\Phi}{\int w^3} - \frac{1}{2}\frac{(\int w^3\Phi)^2}{\int w^4} > 0\,, \tag{C.12}$$

and hence $I_0[\Phi] > 0$ as claimed. If $\int w^3\Phi = 0$, then by Lemma 5.1 (1) of [28], $I_0[\Phi] > 0$. If $\int w^3\Phi \neq 0$, then $I_0[\Phi] > 0$.

https://doi.org/10.1017/S0956792519000305 Published online by Cambridge University Press